ARMY RESEARCH LABORATORY

Resonance Phenomena in Goupillaud-type Media

by George A. Gazonas and Ani P. Velo

ARL-TR-5384 **October 2010**

NOTICES

Disclaimers

The findings in this report are not to be construed as an official Department of the Army position unless so designated by other authorized documents.

Citation of manufacturer's or trade names does not constitute an official endorsement or approval of the use thereof.

Destroy this report when it is no longer needed. Do not return it to the originator.

Army Research Laboratory

Aberdeen Proving Ground, MD 21005-5066

ARL-TR-5384 **October 2010**

Resonance Phenomena in Goupillaud-type Media

George A. Gazonas

Weapons and Materials Research Directorate, ARL

Ani P. Velo

Department of Mathematics and Computer Science, University of San Diego

REPORT DOCUMENTATION PAGE	Form Approved OMB No. 0704-0188

1. REPORT DATE *(DD-MM-YYYY)*	2. REPORT TYPE	3. DATES COVERED (From - To)
October 2010	Final	May 2009-May 2010

4. TITLE AND SUBTITLE
Resonance Phenomena in Goupillaud-type Media

5a. CONTRACT NUMBER

5b. GRANT NUMBER

5c. PROGRAM ELEMENT NUMBER

6. AUTHOR(S)
George A. Gazonas
Ani P. Velo

5d. PROJECT NUMBER
AH84

5e. TASK NUMBER

5f. WORK UNIT NUMBER

7. PERFORMING ORGANIZATION NAME(S) AND ADDRESS(ES)
U.S. Army Research Laboratory
ATTN: RDRL-WMM-B
Aberdeen Proving Ground, MD 21005-5069

8. PERFORMING ORGANIZATION REPORT NUMBER
ARL-TR-5384

9. SPONSORING/MONITORING AGENCY NAME(S) AND ADDRESS(ES)

10. SPONSOR/MONITOR'S ACRONYM(S)

11. SPONSOR/MONITOR'S REPORT NUMBER(S)

12. DISTRIBUTION/AVAILABILITY STATEMENT
Approved for public release; distribution is unlimited.

13. SUPPLEMENTARY NOTES
primary author's email: <george.aristotle.gazonas@us.army.mil>

14. ABSTRACT
The discrete resonance frequency spectrum is derived for an m-layered Goupillaud-type elastic medium subjected to a discrete, time-harmonic forcing function at one end, with the other end fixed. Analytical stress solutions are derived from a global system of recursion relationships using z-transform methods, where the determinant of the resulting global system matrix $|\mathbf{A_m}|$ in the z-space is a palindromic polynomial with real coefficients. The zeros of the palindromic polynomial are distinct and are proven to lie on the unit circle for $1 \leq m \leq 5$. An important result is the physical interpretation that all positive angles, coterminal with the angles corresponding to the zeros of $|\mathbf{A_m}|$ on the unit circle, represent the resonance frequency spectrum for the discrete model. The resonance frequency results are then extended to analytically describe the natural frequency spectrum of a free-fixed m-layered Goupillaud-type medium. The predicted natural frequency spectrum is validated by independently solving a simplified version of the frequency equation involving a transformation of the spatial variable. The natural frequency spectrum is shown to depend only on the layer impedance ratios and is inversely proportional to the equal wave travel time for each layer. A sequence of resonance frequencies for the discrete model is found, which is universal for all multilayered designs with an odd number of layers, and independent of any design parameters.

15. SUBJECT TERMS
wave propagation; z-transform methods; palindromic polynomials with real coefficients; trigonometric sums

16. SECURITY CLASSIFICATION OF:			17. LIMITATION OF ABSTRACT	18. NUMBER OF PAGES	19a. NAME OF RESPONSIBLE PERSON
a. REPORT	b. ABSTRACT	c. THIS PAGE			George A. Gazonas
Unclassified	Unclassified	Unclassified	UU	76	19b. TELEPHONE NUMBER (*Include area code*) 410-306-0863

Standard Form 298 (Rev. 8/98)
Prescribed by ANSI Std. Z39.18

Contents

List of Figures

List of Tables

Acknowledgments

We would like to thank Dr. Steven Segletes for providing the LaTeX style files and the U.S. Army Research Laboratory (ARL) report template for conversion of the original manuscript to ARL report style. Dr. Segletes has also assisted in solving a variety of LaTeX-related format issues in the Table of Contents, Figures, and Appendices.

INTENTIONALLY LEFT BLANK.

1. Introduction

The determination of the natural modes of vibration in layered elastic media is a central problem of geophysics since earthquake-induced free oscillations of the Earth are often used to constrain models of the Earth's interior. Poisson (*1*) was the first to determine the free radial vibrations of a homogeneous sphere, and Lamb (*2*) calculated some of its natural frequencies; the introduction in Love's *Mathematical Treatise of Elasticity* (*3*) provides an historical account of the early developments in this field. It was only with the advent of high-speed computers that planetary-scale vibration problems could be solved with finite, time-dependent sources in compressible, self-gravitating, inhomogeneous, and/or layered oblate spheroids of revolution (*4, 5*). Interestingly, the observed resonance in the free oscillations of the solid Earth, has been attributed to fluid-structure interaction induced by the atmosphere, rather than the cumulative effect of microearthquakes (*6*).

Studies of natural vibrations in elastic media at spatial scales of technological interest focus on resonance in layered structures (*7*), anisotropic elastic bodies (*8*), anisotropic layered crystals (*9, 10*), elastic plates (*11, 12*), periodic media (*13*), laminated and sandwich plates (*14*), composite laminates (*15*), piezoelectric composites (*16*), locally resonant acoustic metamaterials (*17, 18*), and acoustic wave devices that exploit the phenomenon (*19–21*). Thus, it is seen that resonance can enhance the performance of many sensors and devices, yet can damage structures subjected to sustained, temporally periodic loading (*22*).

Although there are numerous works that establish the natural modes of vibration of multilayered media (*23, 24*), and analogous problems for n-segmented strings (*25*) and n-strings (*26*), analytical solutions for the transient resonance response of multilayered media have been limited to analyses involving only a few layers. Churchill (*27*) uses Laplace transform methods to derive the transient resonance response of a free-fixed elastic bar, and notes the presence of the product of a temporal term and time-harmonic function in the solution, which becomes unbounded at large times; similar unbounded behavior is observed in the interaction of a compressible fluid with an elastic plate (*28*). Caviglia and Morro provide closed-form, time-domain expressions for transient waves in a multilayered elastic (possibly anisotropic) medium (*29*). They derive the transient resonance response of a single isotropic elastic layer sandwiched between two half-spaces that is subjected to a temporally periodic sawtooth function, and observe that resonance makes the elastic layer acoustically transparent. A similar two-dimensional problem is studied by Kaplunov and Krynkin (*30*), who examine the influence of layer stiffness and

thickness on the resonance vibrations in a symmetrically point-loaded single layer of elastic material enclosed between two half-spaces. Qiang et al. (*31*) study the natural frequencies of anisotropic multilayers, and illustrate beat phenomena in two and three layer systems using an efficient numerical eigensolution scheme that is based on semi-analytical methods. Exact expressions for the reflection coefficients for a two-dimensional elastic layer overlying an elastic half-space are obtained by Fokina and Fokin (*32*), but the transient response of the system at resonance is not analyzed. Graff presents a general method (*33*) to determine the natural frequencies of composite rods for power ultrasonic applications with a specific solution for a two-rod system. The method can be extended to multilayered systems, but the general problem of determining the natural frequencies with specific geometry and material properties can only be solved using numerical methods. Exact analytical expressions are derivable, however, for the transient resonance response of a multilayered medium if we specialize the medium to be of Goupillaud-type (*34*). The Goupillaud specialization is often used in geophysical applications to model wave propagation in inhomogeneous media (*35*). The present treatment uses a global matrix method that is attributed to Knopoff (*36*), rather than the Thomsen-Haskell transfer matrix formalism (*37, 38*). Since the stresses in the multilayered medium are written in terms of recursion relations that interlace, only half the number of equations are required relative to those in classical global matrix methods (*36*). Finally, Bube and Burridge (*39*) treat the inverse problem of finding the coefficients of a first order 2×2 hyperbolic system related to reflection seismology. In order to numerically solve the continuous initial-boundary-value problem, several difference schemes are applied as discretizations to the corresponding differential equations. The difference scheme IVp, given in equation (3.1.11), pg. 517 of Bube and Burridge (*39*), appears to match our recursive relations for the stress values given in section 2. Our recursive relations are exact for discretely layered media of Goupillaud-type, and the stress solutions that are derived herein using z-transform methods, are then used to determine the resonance response for the discrete model, and subsequently extended to the continuous model.

The remainder of the report is organized as follows. The resonance frequency spectrum for the discrete model is developed in section 2 by generalizing the global system of recursion relations derived in Velo and Gazonas (*40*). Explicit analytical expressions for the stress in a multilayered elastic medium are obtained using z-transform methods and are quantitatively compared with the recursion relation solutions at resonance. These results are then extended in section 3 to analytically describe the natural frequency spectrum of a free-fixed Goupillaud-type strip, also obtained using a generalization of Graff's method. Various applications and interpretations of the frequency results are discussed in section 4. Section 5 summarizes the results, while miscellaneous references and derivations are included in the appendices, including a proof that

the zeros of the palindromic polynomial, representing the determinant of the global system matrix, lie on the unit circle for $1 \leq m \leq 5$.

2. Forced Vibrations and Resonance Frequencies: The Discrete Model

A finite strip made of m-layers of homogeneous elastic materials is considered, where the density and elastic modulus of the material occupying the ith layer are represented by ρ_i and E_i respectively, for $i = 1, \ldots, m$. Using the definition of the wave speed $c = (E/\rho)^{1/2}$, we relate to the ith layer the wave speed c_i for $i = 1, 2, \ldots, m$. The characteristic impedance in the ith layer is given as a product of the material density ρ_i and wave speed c_i, while $\alpha_i = \frac{c_i \rho_i}{c_{i+1}\rho_{i+1}} = \frac{\sqrt{E_i \rho_i}}{\sqrt{E_{i+1}\rho_{i+1}}}$ represents the impedance ratio between layers i and $i+1$ for $i = 1, \ldots, m-1$. The m-layered strip is of Goupillaud-type, which means equal wave travel time for each layer. By replacing the spatial variable x of the wave equation with the new variable $\xi = \int_0^x \frac{ds}{c(s)}$, the problem can be converted to a Goupillaud-type strip with the same length L as the transit time τ through the strip, equal layer lengths of $\frac{\tau}{m}$, and an equal wave travel time of $\frac{\tau}{m}$ for each layer in either direction, which further implies (equal) wave speed of unity for each layer. Here $c = c(s)$ is the piecewise constant wave speed function taking values $c_1, c_2, \ldots, c_m$ in each layer, respectively. In sections 2 and 3, it is shown that the stress values and impedance ratios remain unchanged as a result of this simplification. Therefore, although the spatial variable transformation mentioned previously simplifies the problem, and is used to analyze a Goupillaud-type strip with length τ and unit wave speed in each layer, the results can be applied/interpreted for a Goupillaud-type strip of unequal layer lengths.

In prior work (*40*), the strip was subjected to zero initial conditions, and a Heaviside step in stress loading $p = constant$ at time $t = 0$ at one end, and held fixed at the other end. This is illustrated in figure 1 with $f(n) = p$ for $n \geq 0$. The present work generalizes this system by replacing the Heaviside step in stress loading with a discrete loading function $f(n)$, $n \geq 0$. After transforming the spatial variable x of the wave equation to the new variable $\xi = \int_0^x \frac{ds}{c(s)}$, the initial-boundary

value problem becomes

$$\begin{cases} \frac{\partial^2 u(\xi,t)}{\partial t^2} = \frac{\partial^2 u(\xi,t)}{\partial \xi^2} & \text{for } \frac{(i-1)\tau}{m} < \xi < \frac{i\tau}{m},\ \ i = 1, \ldots, m, \\ \sigma(0,t) = \frac{E_1}{c_1}\frac{\partial u}{\partial \xi}(0,t) = \tilde{E}_1 \frac{\partial u}{\partial \xi}(0,t) = f(n) & \text{for } (n-1)\frac{2\tau}{m} < t < n\frac{2\tau}{m},\ n \geq 1, \\ u(\tau,t) = 0, & \\ u(\xi,0) = \frac{\partial u}{\partial t}(\xi,0) = 0. & \end{cases} \tag{1}$$

The functions u and σ represent the displacement and stress, respectively, while $f(n)$ represents the discrete applied loading. Here, E_i and ρ_i represent the actual material properties for the physical case, while $\tilde{\rho}_i$ and $\tilde{E}_i$ represent the material properties of the ith layer for the simplified case. We will use this notation whenever we want to distinguish the physical case from the simplified case. Having $\tilde{\rho}_i = \tilde{E}_i = \frac{E_i}{c_i} = \sqrt{E_i \rho_i}$, it implies that the impedance ratio $\alpha_i = \frac{\sqrt{E_i \rho_i}}{\sqrt{E_{i+1}\rho_{i+1}}} = \frac{\sqrt{\tilde{E}_i \tilde{\rho}_i}}{\sqrt{\tilde{E}_{i+1}\tilde{\rho}_{i+1}}} = \frac{\tilde{E}_i}{\tilde{E}_{i+1}}$, as well as the stress values $E_1 \frac{\partial u}{\partial x} = \frac{E_1}{c_1}\frac{\partial u}{\partial \xi} = \tilde{E}_1 \frac{\partial u}{\partial \xi}$, remain the same for $i = 1, 2, \ldots, m-1$. As seen in figure 1, the previous coordinates of the boundary and layer interfaces $x_0 = 0$, x_j, and $x_m = L$ are replaced by the new coordinates $\xi_0 = 0$, $\xi_j = \frac{j\tau}{m}$, and $\xi_m = \tau$ for $j = 1, 2, \ldots, m$. The time variable t is represented on the vertical axis and $\frac{\tau}{m}$ represents the (equal) wave travel time for each layer of the m-layered strip in either direction. In figure 1, the stress jump-discontinuities are propagated along the dashed characteristic lines of the wave equation, while the inner vertical solid lines represent the layer interfaces. Due to the zero initial conditions, the stress values below the first characteristic line segment with equation $t = \xi$ for $0 < \xi < \tau$ are zero. Above it, however, the intersection of characteristics with each other and the boundaries splits the region into square subregions. Due to the continuity of stress and displacement at each layer interface, the stress value is constant in each square subregion and is represented by $s_i(n)$ for $i = 1, 2, \ldots, m$ and $n \geq 1$. In a given layer i, the stress values alternate (interlace) between $s_{i-1}(n)$ and $s_i(n)$ for $n = 1, 2, \ldots$, $i = 1, 2, \ldots, m$, and $s_0(n) = f(n)$. When positioned in the middle of the ith or $(i+1)$th layer, the time interval at which $s_i(n)$ is reached is $\frac{4n+2i-3}{2m} < t < \frac{4n+2i-1}{2m}$, as depicted later in figures 2, 3, 4, 6, 8, 9, and 11. Here $n \geq 1$, $i = 0, 1, 2, \ldots, m$, and $s_0(n) = f(n)$.

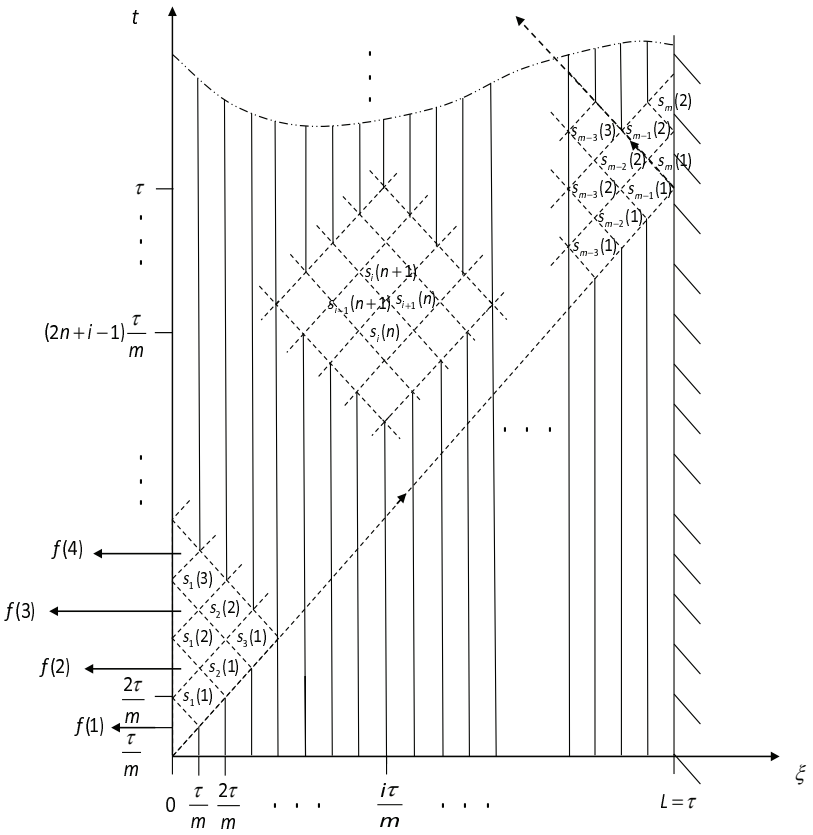

Figure 1. Lagrangian diagram for an elastic strip made of m-layers of equal wave travel time.

From the superposition of the transmitted and reflected waves at the layer interfaces and boundary, a system of coupled first order difference equations for the stress terms was derived in Velo and Gazonas (*40*); the system was then solved using z-transform methods. Herein, we generalize this system of equations by incorporating an arbitrary discrete loading function $f(n)$, $n \geq 0$ which appears in the first line of equation 2:

$$\begin{cases} s_1(n+1) = -s_1(n) + \frac{2\alpha_1}{1+\alpha_1} s_2(n) + \frac{2}{1+\alpha_1} f(n+1), \\ s_2(n+1) = -s_2(n) + \frac{2\alpha_2}{1+\alpha_2} s_3(n) + \frac{2}{1+\alpha_2} s_1(n+1), \\ \dots \\ s_i(n+1) = -s_i(n) + \frac{2\alpha_i}{1+\alpha_i} s_{i+1}(n) + \frac{2}{1+\alpha_i} s_{i-1}(n+1), \\ \dots \\ s_{m-1}(n+1) = -s_{m-1}(n) + \frac{2\alpha_{m-1}}{1+\alpha_{m-1}} s_m(n) + \frac{2}{1+\alpha_{m-1}} s_{m-2}(n+1), \\ s_m(n+1) = -s_m(n) + 2 s_{m-1}(n+1), \end{cases} \tag{2}$$

subject to zero-stress initial conditions $s_i(0) = 0$ for $1 \leq i \leq m$. Here $n \geq 0$ is a suitable time index and $s_i(n)$ represent the stress terms for $1 \leq i \leq m$ (see figure 1). The discrete function $f(n)$, $n \geq 0$, represents the stress loading applied at $\xi = 0$. Notice that by applying the limiting condition $\alpha_i \to 0$ to the recursive relation $s_i(n+1) = -s_i(n) + \frac{2\alpha_i}{1+\alpha_i} s_{i+1}(n) + \frac{2}{1+\alpha_i} s_{i-1}(n+1)$ for $i = m$, we recover the last line of equation 2, corresponding to the fixed end. A similar system of difference equations may be obtained for other initial and boundary conditions. For example, a free-free multilayered system can be studied by setting the last line in equation 2 to $s_m(n) = s_m(0) = 0$, and a multilayer on a half-space can be obtained using $s_m(n+1) = s_{m-1}(n+1)$, and the rest of the equations for $1 \leq i < m$ remain the same.

Equation 2 can then be solved using z-transform methods. Indeed, due to the zero-stress initial conditions $s_i(0) = 0$ for $1 \leq i \leq m$, the z-transform[1] of $s_i(n+1)$ becomes

$$Z(s_i(n+1)) = zS_i(z) - zs_i(0) = zS_i(z), \tag{3}$$

where $S_i(z)$ is the z-transform of $s_i(n)$, while

$$Z(f(n+1)) = zF(z) - zf(0) = z(F(z) - f(0)), \tag{4}$$

where $F(z)$ is the z-transform of $f(n)$. As a result, the z-transform of equation 2 is expressed as

$$\begin{cases} zS_1(z) = -S_1(z) + \frac{2\alpha_1}{1+\alpha_1} S_2(z) + \frac{2}{1+\alpha_1} z(F(z) - f(0)), \\ zS_2(z) = -S_2(z) + \frac{2\alpha_2}{1+\alpha_2} S_3(z) + \frac{2}{1+\alpha_2} zS_1(z), \\ \dots \\ zS_i(z) = -S_i(z) + \frac{2\alpha_i}{1+\alpha_i} S_{i+1}(z) + \frac{2}{1+\alpha_i} zS_{i-1}(z), \\ \dots \\ zS_{m-1}(z) = -S_{m-1}(z) + \frac{2\alpha_{m-1}}{1+\alpha_{m-1}} S_m(z) + \frac{2}{1+\alpha_{m-1}} zS_{m-2}(z), \\ zS_m(z) = -S_m(z) + 2zS_{m-1}(z). \end{cases} \tag{5}$$

After reorganizing the terms in equation 5, the linear system is written in matrix-vector form as

$$\mathbf{A_m}\tilde{\mathbf{x}}_\mathbf{m} = \tilde{\mathbf{b}}_\mathbf{m}, \tag{6}$$

[1]The definition for the z-transform of $g(n)$, $n \geq 0$, is $Z(g(n)) = G(z) = \sum_{n=0}^{\infty} g(n) z^{-n}$ for $|z| > R$ in the complex plane (see Jury (*41*)).

where $\mathbf{A_m}$ is a tridiagonal matrix given as

$$\mathbf{A_m} = \begin{bmatrix} z+1 & -\eta_1\alpha_1 & 0 & \cdots & 0 & 0 & 0 & 0 \\ -\eta_2 z & z+1 & -\eta_2\alpha_2 & 0 & \cdots & 0 & 0 & 0 \\ 0 & -\eta_3 z & z+1 & -\eta_3\alpha_3 & 0 & \cdots & 0 & 0 \\ \ddots & \ddots & \ddots & & \ddots & \ddots & \ddots & \\ 0 & 0 & 0 & \cdots & 0 & -\eta_{m-1}z & z+1 & -\eta_{m-1}\alpha_{m-1} \\ 0 & 0 & 0 & \cdots & 0 & 0 & -\eta_m z & z+1 \end{bmatrix}_{m\times m}, \quad (7)$$

while

$$\tilde{\mathbf{x}}_\mathbf{m} = \begin{bmatrix} S_1(z) \\ S_2(z) \\ \vdots \\ S_m(z) \end{bmatrix}_{m\times 1}, \ \tilde{\mathbf{b}}_\mathbf{m} = \begin{bmatrix} \eta_1 z(F(z)-f(0)) \\ 0 \\ \vdots \\ 0 \end{bmatrix}_{m\times 1}, \ \eta_i = \tfrac{2}{1+\alpha_i} \text{ for } i = 1,\ldots,m-1, \eta_m = 2. \quad (8)$$

Due to the sparseness of $\tilde{\mathbf{b}}_\mathbf{m}$, the solution of the linear system in equation 6 is

$$\tilde{\mathbf{x}}_\mathbf{m} = {\mathbf{A_m}}^{-1}\tilde{\mathbf{b}}_\mathbf{m} = \tfrac{\eta_1 z(F(z)-f(0))}{|\mathbf{A_m}|}\begin{bmatrix} (-1)^{1+1}|\mathbf{A_{1,1}}| \\ (-1)^{1+2}|\mathbf{A_{1,2}}| \\ \vdots \\ (-1)^{1+m}|\mathbf{A_{1,m}}| \end{bmatrix} = \tfrac{\eta_1 z(F(z)-f(0))}{|\mathbf{A_m}|}\begin{bmatrix} |\mathbf{A_{1,1}}| \\ -|\mathbf{A_{1,2}}| \\ \vdots \\ (-1)^{1+m}|\mathbf{A_{1,m}}| \end{bmatrix}. \quad (9)$$

Here $|\mathbf{A_m}|$ is the determinant of $\mathbf{A_m}$, $\mathbf{A_{1,i}}$ for $i = 1,\ldots,m$ are minors of $\mathbf{A_m}$, and $|\mathbf{A_{1,i}}|$ are their corresponding determinants. The following recursive relation (see e.g., Muir (*42*)) holds

$$|\mathbf{A_m}| = (z+1)|\mathbf{A_{m-1}}| - \eta_1\eta_2\alpha_1 z|\mathbf{A_{m-2}}|, \quad (10)$$

where $\mathbf{A_m}$ corresponds to the m-layered strip with impedance ratios $\alpha_1, \alpha_2, \ldots, \alpha_{m-1}$; and $\mathbf{A_{m-1}}$ corresponds to the remaining $(m-1)$-layered strip with impedance ratios $\alpha_2, \alpha_3, \ldots, \alpha_{m-1}$, obtained after the removal of the first layer from the m-layered strip; $\mathbf{A_{m-2}}$ corresponds to the remaining $(m-2)$-layered strip with impedance ratios $\alpha_3, \ldots, \alpha_{m-1}$, obtained after the removal of the first two layers from the m-layered strip. One can derive by induction that the determinant $|\mathbf{A_m}|$ is a palindromic polynomial with real coefficients, i.e., the coefficients in front of z^{m-j} and z^j are real and equal to each-other for $j = 0, \ldots, m$ and $m \geq 1$:

$$|\mathbf{A_m}| = \begin{cases} z^m + a_{m,1}z^{m-1} + a_{m,2}z^{m-2} + \cdots + a_{m,\frac{m}{2}-1}z^{\frac{m}{2}+1} + a_{m,\frac{m}{2}}z^{\frac{m}{2}} + \\ +a_{m,\frac{m}{2}-1}z^{\frac{m}{2}-1} + \cdots + a_{m,2}z^2 + a_{m,1}z + 1, \qquad \text{for } m\text{-even}, \\ \\ (z+1)[z^{m-1} + b_{m,1}z^{m-2} + \cdots + b_{m,\frac{m-1}{2}-1}z^{\frac{m-1}{2}+1} + b_{m,\frac{m-1}{2}}z^{\frac{m-1}{2}} + \\ +b_{m,\frac{m-1}{2}-1}z^{\frac{m-1}{2}-1} + \cdots + b_{m,2}z^2 + b_{m,1}z + 1], \qquad \text{for } m\text{-odd}. \end{cases} \tag{11}$$

The complex roots of a polynomial with real coefficients occur in conjugate pairs, and if the coefficients are palindromic, then the roots occur in inverse pairs. Since the inverse pairing is not necessarily the same as the conjugate pairing, if a root's inverse is not its conjugate, then it must be one of a set of four related roots that satisfy a palindromic quartic with real coefficients. As a result, each palindromic polynomial of even degree in equation 11 is expected to factor into quadratic and quartic palindromes with real coefficients. In appendix B, the quadratic and quartic factors of $|\mathbf{A_m}|$ for $1 \leq m \leq 5$ are shown to satisfy the necessary and sufficient conditions for all their roots to be distinct (complex conjugate), and on the unit circle. As a result, all the zeros of $|\mathbf{A_m}|$ for $1 \leq m \leq 5$ are on the unit circle, and their corresponding angles are provided in appendix D.

In this report, we only consider m-layered designs for which all the zeros of $|\mathbf{A_m}|$ are distinct, have no multiples, and are on the unit circle. Based on the results from appendix B, this class of designs is not empty. Under this assumption, $z_k = e^{\mathcal{I}\theta_k} = \cos\theta_k + \mathcal{I}\sin\theta_k$, and $z_k^{-1} = \bar{z_k} = e^{-\mathcal{I}\theta_k} = \cos\theta_k - \mathcal{I}\sin\theta_k$, where $\bar{z_k}$ is the complex conjugate of z_k and $1 \leq k \leq \lfloor \frac{m}{2} \rfloor$. From the fact that

$$z_k + z_k^{-1} = z_k + \bar{z_k} = 2\cos\theta_k, \tag{12}$$

a newly factored representation of $|\mathbf{A_m}|$ is obtained, with linear factor $(z+1)$ for m-odd, and only

palindromic quadratics with real coefficients involving the cosines of the angles $\theta_1, \theta_2, \ldots, \theta_{\lfloor \frac{m}{2} \rfloor}$,

$$|\mathbf{A_m}| = \begin{cases} \prod_{k=1}^{\lfloor \frac{m}{2} \rfloor} [z^2 - 2z\cos\theta_k + 1] & \text{for } m \text{ even}, \\ (z+1) \prod_{k=1}^{\lfloor \frac{m}{2} \rfloor} [z^2 - 2z\cos\theta_k + 1] & \text{for } m \text{ odd}. \end{cases} \tag{13}$$

Based on the factorization of the determinant $|\mathbf{A_m}|$ given in equation 13, for any m-layered design, if there are m distinct roots on the unit circle, then there are m distinct angles. The angles $\{\pm\theta_k\}_{k=1}^{\frac{m}{2}}$ correspond to the roots $z = e^{\pm\mathcal{I}\theta_k}$ for m even, while the angles $\theta_0 = \pi$, $\{\pm\theta_k\}_{k=1}^{\lfloor \frac{m}{2} \rfloor}$ correspond to the roots $z = e^{\mathcal{I}\theta_0} = -1$ and $z = e^{\pm\mathcal{I}\theta_k}$, respectively, for m odd. The $\lfloor \frac{m}{2} \rfloor$ essential angles $0 < \theta_k < \pi$ for $k = 1, \ldots, \lfloor \frac{m}{2} \rfloor$ were referred to as the base angles in Velo and Gazonas (*40*). The equations for the angles $\theta_0 = \pi$ and $\{\theta_k\}_{k=1}^{\lfloor \frac{m}{2} \rfloor}$ in terms of the design parameters (combinations of the impedance ratios) can be derived from the condition:

$$|\mathbf{D_m}| = 0. \tag{14}$$

The definition for the matrix $\mathbf{D_m}$ as well as the angle-design parameter equations for up to five layers are included in appendices C–D.

In the rest of this section, we prove that the resonance frequency spectrum for the discrete model consists of all the positive angles coterminal with $\theta_0 = \pi$ or $\{\pm\theta_k\}_{k=1}^{\lfloor \frac{m}{2} \rfloor}$, as shown below

$$\begin{cases} \tilde{\omega}_{l_0} = \theta_0 + 2l_0\pi = (2l_0+1)\pi \text{ (for } m \text{ odd only)}, & \\ \tilde{\omega}_{l_1,k} = \theta_k + 2l_1\pi, & l_0, l_1, l_2 = 0, 1, 2\ldots, \\ \tilde{\omega}_{l_2,k} = -\theta_k + 2(l_2+1)\pi, & k = 1, \ldots, \lfloor \frac{m}{2} \rfloor. \end{cases} \tag{15}$$

Equivalently, the resonance frequency $\tilde{\omega}$ is expected to satisfy one of the following relations:

$$\begin{cases} \cos\tilde{\omega} = -1 & \text{(for } m \text{ odd only)}, \\ \cos\tilde{\omega} = \cos\theta_k & \text{for } k = 1, \ldots, \lfloor \frac{m}{2} \rfloor. \end{cases} \tag{16}$$

Since the degree of $|\mathbf{A_m}|$ is m and the degree of its minors $|\mathbf{A_{1,i}}|$ is $m-1$, for $i = 1, 2, \ldots, m$, the substitution of equation 13 into equation 9 results in the following expansion of the components $\tilde{\mathbf{x}}_\mathbf{m}(i)$ of $\tilde{\mathbf{x}}_\mathbf{m}$ into partial fractions:

$$
\begin{aligned}
\tilde{\mathbf{x}}_{\mathbf{m}}(i) &= z(F(z)-f(0))\left[\frac{\eta_1(-1)^i|\mathbf{A_{1,i}}|}{|\mathbf{A_m}|}\right] \\
&= z(F(z)-f(0))\left[\frac{b_{i,0}}{z+1}+\sum_{k=1}^{\lfloor\frac{m}{2}\rfloor}\frac{a^*_{i,k}z+b^*_{i,k}}{z^2-2z\cos\theta_k+1}\right] \\
&= (F(z)-f(0))\left[\frac{b_{i,0}z}{z+1}+\sum_{k=1}^{\lfloor\frac{m}{2}\rfloor}\frac{a^*_{i,k}z^2+b^*_{i,k}z}{z^2-2z\cos\theta_k+1}\right],
\end{aligned}
\tag{17}
$$

where $b_{i,0}=0$ for m even and $i=1,2,\ldots,m$. Applying the inverse z-transform, one can derive that

$$
\begin{aligned}
&Z^{-1}\left[\frac{b_{i,0}z}{z+1}+\sum_{k=1}^{\lfloor\frac{m}{2}\rfloor}\frac{a^*_{i,k}z^2+b^*_{i,k}z}{z^2-2z\cos\theta_k+1}\right]=Z^{-1}\left[\frac{b_{i,0}\cdot z}{z+1}+\sum_{k=1}^{\lfloor\frac{m}{2}\rfloor}\left(\frac{a_{i,k}\cdot z(z-\cos\theta_k)}{z^2-2z\cos\theta_k+1}+\frac{b_{i,k}\cdot z\sin\theta_k}{z^2-2z\cos\theta_k+1}\right)\right] \\
&=b_{i,0}(-1)^n+\sum_{k=1}^{\lfloor\frac{m}{2}\rfloor}a_{i,k}\cos(n\theta_k)+b_{i,k}\sin(n\theta_k),
\end{aligned}
\tag{18}
$$

for the following choices of the coefficients and $i=1,2,\ldots,m$,

$$
a_{i,k}=a^*_{i,k},\ b_{i,k}=\frac{a^*_{i,k}\cos\theta_k+b^*_{i,k}}{\sin\theta_k}\ \text{for}\ k=1,\ldots,\lfloor\frac{m}{2}\rfloor. \tag{19}
$$

From the fact that $0<\theta_k<\pi$ it follows that $\sin\theta_k\neq 0$ for all $k=1,\ldots,\lfloor\frac{m}{2}\rfloor$. As a result, after applying the inverse z-transform to equation 17 and based on equation 18, a general representation for the stress terms in equation 2 is obtained,

$$
\begin{aligned}
s_i(n)=Z^{-1}(\tilde{\mathbf{x}}_{\mathbf{m}}(i))= \;& f(n)*\left[b_{i,0}(-1)^n+\sum_{k=1}^{\lfloor\frac{m}{2}\rfloor}a_{i,k}\cos(n\theta_k)+b_{i,k}\sin(n\theta_k)\right] \\
& -f(0)\cdot\left[b_{i,0}(-1)^n+\sum_{k=1}^{\lfloor\frac{m}{2}\rfloor}a_{i,k}\cos(n\theta_k)+b_{i,k}\sin(n\theta_k)\right],
\end{aligned}
\tag{20}
$$

where operation $*$ means convolution, $i=1,2,\ldots m$, and $n\geq 0$. The stress representation previously derived in Velo and Gazonas (*40*) can now be recovered for the special choice of loading $f(n)=p$ for $n\geq 0$ (see appendix A for further details). The stress representation in equation 20 involves trigonometric sums which relate to the Chebyshev polynomials of the first and second kind (see subsection 4.4).

In the work that follows, we use equations 17–18 to obtain stress solutions when a harmonic forcing function of the form $f(n) = \sin(n\tilde{\omega})$ with $f(0) = 0$ and $n \geq 0$ is applied, unless mentioned otherwise. A similar approach can be used for a harmonic forcing function of the form $f(n) = \cos(n\tilde{\omega})$ for $n \geq 0$. As discussed in Proakis and Manolakis (*43*), the nature of time (continuous or discrete) is expected to affect the nature of the frequency. The frequency for the analog (continuous) time signal is related to the frequency of the digital (discrete) time signal through a linear transformation involving the time step or the so-called sampling interval. There is a linear transformation in frequency

$$\tilde{\omega} = \frac{2\tau}{m}\omega, \tag{21}$$

from the continuous forcing function with frequency ω to the discrete forcing function with frequency $\tilde{\omega}$, and time step $\frac{2\tau}{m}$:

$$\sin(t\omega) = \sin\left(\frac{t}{\frac{2\tau}{m}} \cdot \frac{2\tau}{m}\omega \right) \rightarrow \sin\left(\lceil \frac{t}{\frac{2\tau}{m}} \rceil \cdot \frac{2\tau}{m}\omega \right) = \sin\left(n \cdot \frac{2\tau}{m}\omega \right) = \sin(n\tilde{\omega}). \tag{22}$$

As seen in figure 1, $t \geq 0$ represents the time variable, $n = \lceil \frac{t}{\frac{2\tau}{m}} \rceil = 0, 1, 2, \ldots$ represents a time-related index, τ represents the wave transit time through the layered strip, and m represents the number of layers.

For the choice of $f(n) = \sin(n\tilde{\omega})$, $n \geq 0$, unless mentioned otherwise, we analytically prove the equivalent equations 15 and 16, and validate them through various numerical experiments. Substituting $f(0) = 0$ into equation 17, and

$$F(z) = Z(f(n)) = Z(\sin(n\tilde{\omega})) = \frac{z\sin(\tilde{\omega})}{(z^2 - 2z\cos\tilde{\omega} + 1)}, \tag{23}$$

after using equation 18, it can be shown that

$$\begin{aligned} s_i(n) &= Z^{-1}(\tilde{\mathbf{x}}_{\mathbf{m}}(i)) \\ &= Z^{-1}\left[\frac{z\sin(\tilde{\omega})}{(z^2-2z\cos\tilde{\omega}+1)} \cdot \left(\frac{b_{i,0}z}{z+1} + \sum_{k=1}^{\lfloor \frac{m}{2} \rfloor} \frac{a^*_{i,k}z^2+b^*_{i,k}z}{z^2-2z\cos\theta_k+1} \right) \right] \\ s_i(n) &= b_{i,0}Z^{-1}\left[\frac{z^2\sin(\tilde{\omega})}{(z^2-2z\cos\tilde{\omega}+1)(z+1)} \right] + \sum_{k=1}^{\lfloor \frac{m}{2} \rfloor} Z^{-1}\left[\frac{z\sin(\tilde{\omega})\cdot(a^*_{i,k}z^2+b^*_{i,k}z)}{(z^2-2z\cos\theta_k+1)(z^2-2z\cos\tilde{\omega}+1)} \right], \end{aligned} \tag{24}$$

or equivalently,

$$s_i(n) = b_{i,0}Z^{-1}\left[\frac{z^2\sin(\tilde{\omega})}{(z^2-2z\cos\tilde{\omega}+1)(z+1)} \right] + \sum_{k=1}^{\lfloor \frac{m}{2} \rfloor} Z^{-1}\left[\frac{z\sin(\tilde{\omega})\cdot(a^*_{i,k}z^2+b^*_{i,k}z)}{(z^2-2z\cos\theta_k+1)(z^2-2z\cos\tilde{\omega}+1)} \right]. \tag{25}$$

In the subsections that follow, we calculate the inverse z-transform of both expressions in equation 25 in order to derive the stress formulas at resonance and non-resonance frequencies.

2.1 Stress Solutions at Non-resonance Frequencies

Here we show that the values of the driving frequency $\tilde{\omega}$, which satisfy $\cos\tilde{\omega} \neq -1 = \cos\theta_0$ (for m odd) and $\cos\tilde{\omega} \neq \cos\theta_k$ for all $k = 1, \ldots, \lfloor \frac{m}{2} \rfloor$, represent non-resonance frequency values. In the set of real numbers, this set of frequency values is the complement of the set of values identified in equation 16. We begin by finding the inverse z-transform of the two expressions given in equations 27 and 29.

When $\cos\tilde{\omega} \neq -1$, the partial fraction expansion

$$\begin{aligned} \tfrac{z^2\sin(\tilde{\omega})}{(z^2-2z\cos\tilde{\omega}+1)(z+1)} &= \tfrac{\sin\tilde{\omega}}{2(1+\cos\tilde{\omega})} \cdot \left[\tfrac{z^2+z}{z^2-2z\cos\tilde{\omega}+1} - \tfrac{z}{z+1} \right] \\ &= \tfrac{1}{2(1+\cos\tilde{\omega})} \cdot \left[\tfrac{z(z-\cos\tilde{\omega})\sin\tilde{\omega}}{z^2-2z\cos\tilde{\omega}+1} + \tfrac{z\sin\tilde{\omega}(1+\cos\tilde{\omega})}{z^2-2z\cos\tilde{\omega}+1} - \sin\tilde{\omega}\tfrac{z}{z+1} \right], \end{aligned} \tag{26}$$

implies that

$$Z^{-1}\left[\tfrac{z^2\sin(\tilde{\omega})}{(z^2-2z\cos\tilde{\omega}+1)(z+1)} \right] = \tfrac{\sin\tilde{\omega}}{2(1+\cos\tilde{\omega})}\cos(n\tilde{\omega}) + \tfrac{1}{2}\sin(n\tilde{\omega}) - \tfrac{\sin\tilde{\omega}}{2(1+\cos\tilde{\omega})}(-1)^n. \tag{27}$$

When $\cos\tilde{\omega} \neq \cos\theta$, the partial fraction expansion,

$$\begin{aligned} \frac{z\sin\tilde{\omega}(az^2+bz)}{(z^2-2z\cos\tilde{\omega}+1)(z^2-2z\cos\theta+1)} &= \frac{Az(z-\cos\tilde{\omega})}{z^2-2z\cos\tilde{\omega}+1} + \frac{Bz\sin\tilde{\omega}}{z^2-2z\cos\tilde{\omega}+1} \\ &\quad + \frac{Cz(z-\cos\theta)}{z^2-2z\cos\theta+1} + \frac{Dz\sin\theta}{z^2-2z\cos\theta+1}, \end{aligned} \tag{28}$$

implies that

$$\begin{aligned} Z^{-1}\left[\frac{z\sin\tilde{\omega}(az^2+bz)}{(z^2-2z\cos\tilde{\omega}+1)(z^2-2z\cos\theta+1)} \right] &= A\cos(n\tilde{\omega}) + B\sin(n\tilde{\omega}) \\ &\quad + C\cos(n\theta) + D\sin(n\theta), \end{aligned} \tag{29}$$

where $A = -C = \frac{a\sin\tilde{\omega}}{2(\cos\tilde{\omega}-\cos\theta)}$, $B = \frac{a\cos\tilde{\omega}+b}{2(\cos\tilde{\omega}-\cos\theta)}$, and $D = -\frac{(a\cos\theta+b)\sin\tilde{\omega}}{2\sin\theta(\cos\tilde{\omega}-\cos\theta)}$. Substituting the results from equations 27 and 29 into equation 25, the following stress solutions for

$\cos\tilde{\omega} \neq -1 = \cos\theta_0$ and $\cos\tilde{\omega} \neq \cos\theta_k$ for all $k = 1, \ldots, \lfloor \frac{m}{2} \rfloor$ are obtained:

$$\begin{aligned} s_i(n) &= -\tfrac{b_{i,0}\sin\tilde{\omega}}{2(1+\cos\tilde{\omega})}(-1)^n + \left[\tfrac{b_{i,0}\sin\tilde{\omega}}{2(1+\cos\tilde{\omega})} + \sum_{k=1}^{\lfloor \frac{m}{2} \rfloor} A_{i,k} \right] \cos(n\tilde{\omega}) \\ &\quad + \left[\tfrac{b_{i,0}}{2} + \sum_{k=1}^{\lfloor \frac{m}{2} \rfloor} B_{i,k} \right] \sin(n\tilde{\omega}) + \sum_{k=1}^{\lfloor \frac{m}{2} \rfloor} C_{i,k}\cos(n\theta_k) + \sum_{k=1}^{\lfloor \frac{m}{2} \rfloor} D_{i,k}\sin(n\theta_k), \end{aligned} \tag{30}$$

where

$$A_{i,k} = -C_{i,k} = \tfrac{a^*_{i,k}\sin\tilde{\omega}}{2(\cos\tilde{\omega}-\cos\theta_k)}, B_{i,k} = \tfrac{a^*_{i,k}\cos\tilde{\omega}+b^*_{i,k}}{2(\cos\tilde{\omega}-\cos\theta_k)}, D_{i,k} = -\tfrac{(a^*_{i,k}\cos\theta_k+b^*_{i,k})\sin\tilde{\omega}}{2\sin\theta_k(\cos\tilde{\omega}-\cos\theta_k)}. \tag{31}$$

As before, $b_{i,0} = 0$ when the number of layers m is even. For a given value of $\tilde{\omega}$, the stress solutions in equation 30, including all the coefficients and angles θ_k for $k = 1, \ldots, \lfloor \frac{m}{2} \rfloor$, can be also expressed in terms of the impedance ratios only (see equations 6–9, 14, and appendices D and E).

Given that $0 < \theta_k < \pi$ implies that $\sin\theta_k \neq 0$ for all $k = 1, \ldots, \lfloor \frac{m}{2} \rfloor$. This, together with the fact that $\cos\tilde{\omega} \neq -1$ and $\cos\tilde{\omega} \neq \cos\theta_k$ for all $k = 1, \ldots, \lfloor \frac{m}{2} \rfloor$, implies that the coefficients in the stress solutions are always bounded (see equations 30–31). Therefore, for a given m-layered design and driving frequency $\tilde{\omega}$, the stress solutions in equations 30 given by trigonometric sums of sines and cosines are bounded. However, as $\cos\tilde{\omega}$ approaches $-1 = \cos\theta_0$ (for m odd) or any of the $\cos\theta_k$ values, $k = 1, \ldots, \lfloor \frac{m}{2} \rfloor$, the denominators of some coefficients of the stress solutions in equations 30–31 get close to zero, allowing these solutions to take larger values and approach resonance.

2.2 Stress Solutions at Resonance Frequencies

The stress solutions in equation 30 suggest that the driving frequencies $\tilde{\omega}$ identified in equation 16 are resonance frequencies. Here we prove equation 16 and its equivalent form equation 15, by deriving the stress solutions at the expected resonance frequencies, demonstrating that these solutions grow without bound over time.

2.2.1 Case I: $\cos\tilde{\omega} = -1 = \cos\theta_0$ (for m odd only)

The fact that $\cos(\tilde{\omega}) = -1$ or equivalently that $\tilde{\omega}$ takes values $\tilde{\omega}_{l_0} = (2l_0 + 1)\pi$ for $l_0 = 0, 1, 2\ldots$, implies that $f(n) = \sin(n\tilde{\omega}) = \sin(n\pi) = 0$ for all $n \geq 0$. As a result, due to the zero input in loading we are unable to detect resonance, as confirmed by equation 20. However, by choosing $f(n) = \cos(n\tilde{\omega}) = \cos(n\pi)$ we overcome this obstacle. Based on equations 17–20, we expect

any unbounded stress terms to come from

$$F(z) \cdot \left[\frac{b_{i,0} z}{z+1} + \sum_{k=1}^{\lfloor \frac{m}{2} \rfloor} \frac{a_{i,k}^* z^2 + b_{i,k}^* z}{z^2 - 2z\cos\theta_k + 1} \right], \tag{32}$$

after the inverse z-transform is applied. Here $F(z) = Z(f(n)) = Z(\cos((n\pi)) = \frac{z}{z+1}$, which after substituting into equation 32, gives

$$\begin{aligned} &\tfrac{z}{z+1} \cdot \left[\tfrac{b_{i,0} z}{z+1} + \sum_{k=1}^{\lfloor \frac{m}{2} \rfloor} \tfrac{a_{i,k}^* z^2 + b_{i,k}^* z}{z^2 - 2z\cos\theta_k + 1} \right] = \tfrac{b_{i,0} z^2}{(z+1)^2} + \sum_{k=1}^{\lfloor \frac{m}{2} \rfloor} \tfrac{z \cdot (a_{i,k}^* z^2 + b_{i,k}^* z)}{(z+1)(z^2 - 2z\cos\theta_k + 1)} \\ &= \tfrac{b_{i,0} z^2}{(z+1)^2} + \sum_{k=1}^{\lfloor \frac{m}{2} \rfloor} \tfrac{a_{i,k}^* z^2 + b_{i,k}^* z}{z^2 - 2z\cos\theta_k + 1} - \sum_{k=1}^{\lfloor \frac{m}{2} \rfloor} \tfrac{a_{i,k}^* z^2 + b_{i,k}^* z}{(z+1)(z^2 - 2z\cos\theta_k + 1)}. \end{aligned} \tag{33}$$

Furthermore, for the last sum above, we have that

$$\begin{aligned} &\sum_{k=1}^{\lfloor \frac{m}{2} \rfloor} \tfrac{a_{i,k}^* z^2 + b_{i,k}^* z}{(z+1)(z^2 - 2z\cos\theta_k + 1)} \\ &= \sum_{k=1}^{\lfloor \frac{m}{2} \rfloor} \tfrac{a_{i,k}^*}{\sin\theta_k} \cdot \tfrac{z^2 \sin\theta_k}{(z+1)(z^2 - 2z\cos\theta_k + 1)} + \sum_{k=1}^{\lfloor \frac{m}{2} \rfloor} b_{i,k}^* \cdot \tfrac{z}{(z+1)(z^2 - 2z\cos\theta_k + 1)} \\ &= \sum_{k=1}^{\lfloor \frac{m}{2} \rfloor} \tfrac{a_{i,k}^*}{\sin\theta_k} \cdot \tfrac{z^2 \sin\theta_k}{(z+1)(z^2 - 2z\cos\theta_k + 1)} + \sum_{k=1}^{\lfloor \frac{m}{2} \rfloor} \tfrac{b_{i,k}^*}{2\cos\theta_k} \cdot \left[\tfrac{z}{z+1} + \tfrac{-z^2 + (1+2\cos\theta_k) z}{z^2 - 2z\cos\theta_k + 1} \right]. \end{aligned} \tag{34}$$

Applying the inverse z-transform to the sums in equations 33–34 and using equations 18 and 27, we conclude that the only term in equation 33 that generates unbounded stress values is $\frac{b_{i,0} z^2}{(z+1)^2}$ for $b_{i,0} \neq 0$, due to the fact that

$$Z^{-1}\left[\frac{b_{i,0} z^2}{(z+1)^2} \right] = b_{i,0} \cdot W_n(-1) = b_{i,0}(-1)^n (n+1). \tag{35}$$

Here $W_n(y)$ represents the Chebyshev polynomial of the second kind evaluated at $y = -1$. The presence of resonance for the choice of frequency values $\tilde{\omega}_{l_0} = (2l_0 + 1)\pi$, $l_0 = 0, 1, 2, \ldots,$ proves that they are part of the resonance frequency spectrum identified in equation 15. Notice that the resonance frequency spectrum $\tilde{\omega}_{l_0} = (2l_0 + 1)\pi$ for $l_0 = 0, 1, 2, \ldots$ **is universal for all the designs with an odd number of layers as it is independent of any design parameters (e.g., impedance ratios)**. This is illustrated in figure 2 for the 7- and 11-layer case and later on in figure 8 for the 3-layer case.

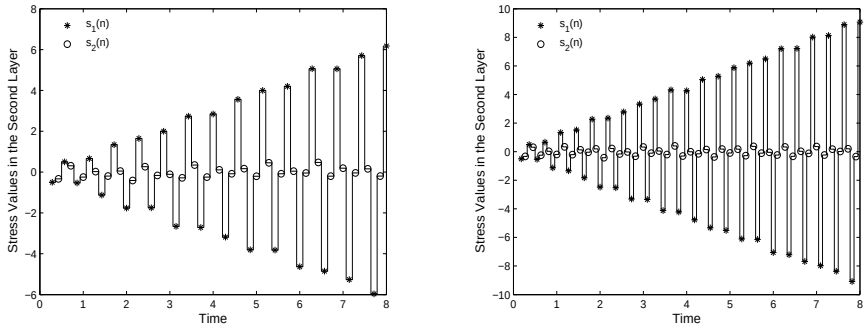

(a) (b)

Figure 2. Stress time history for a layered strip with impedance ratios $\alpha_1 = 3$, $\alpha_2 = 2$, $\alpha_3 = 1.5$, $\alpha_4 = 2.2$, $\alpha_5 = 0.3$, $\alpha_6 = 1.7$, $\alpha_7 = 1.4$, $\alpha_8 = 3.1$, $\alpha_9 = 0.8$, and $\alpha_{10} = 4$ as applicable; $\tau = 1$ and loading $f(n) = \cos(n\tilde{\omega})$ applied at $\xi = 0$ for $\tilde{\omega} = \pi$. (a) The middle of the second layer of a 7-layered strip located at $\xi = 3/14$. (b) The middle of the second layer of an 11-layered strip located at $\xi = 3/22$.

2.2.2 Case II: $\cos\tilde{\omega} = \cos\theta_{k^*}$

The following expansion

$$\frac{z\sin\theta(az^2+bz)}{(z^2-2z\cos\theta+1)^2} = \frac{\tilde{A}z[-2z+(1+z^2)\cos\theta}{(z^2-2z\cos\theta+1)^2}] + \frac{\tilde{B}z(z^2-1)\sin\theta}{(z^2-2z\cos\theta+1)^2} + \frac{\tilde{C}z\sin\theta}{z^2-2z\cos\theta+1} \tag{36}$$

implies that

$$Z^{-1}\left[\frac{z\sin\theta(az^2+bz)}{(z^2-2z\cos\theta+1)^2}\right] = \tilde{A}\cdot n\cos(n\theta) + \tilde{B}\cdot n\sin(n\theta) + \tilde{C}\sin(n\theta), \tag{37}$$

where $\tilde{A} = -\frac{(a\cos\theta+b)}{2\sin\theta}$, $\tilde{B} = \frac{a}{2}$, and $\tilde{C} = \frac{a+b\cos\theta}{2\sin^2\theta}$.

2.2.3 Case II.a.: $\sin\tilde{\omega} = \sin\theta_{k^*}$

Applying equations 27, 29, and 37 to equation 25, the following stress solutions for the frequency spectrum $\tilde{\omega}_{l_1,k^*} = \theta_{k^*} + 2l_1\pi$, $l_1 = 0, 1, 2, \ldots$ are obtained,

$$
\begin{aligned}
s_i(n) \;=\; & -\tfrac{b_{i,0}\sin\theta_{k^*}}{2(1+\cos\theta_{k^*})}(-1)^n + \left[\tfrac{b_{i,0}\sin\theta_{k^*}}{2(1+\cos\theta_{k^*})} + n\tilde{A}_{i,k^*} + \sum_{k=1,k\neq k^*}^{\lfloor\frac{m}{2}\rfloor} A_{i,k}\right]\cos(n\theta_{k^*}) \\
& + \left[\tfrac{b_{i,0}}{2} + n\tilde{B}_{i,k^*} + \tilde{C}_{i,k^*} + \sum_{k=1,k\neq k^*}^{\lfloor\frac{m}{2}\rfloor} B_{i,k}\right]\sin(n\theta_{k^*}) \\
& + \sum_{k=1,k\neq k^*}^{\lfloor\frac{m}{2}\rfloor} C_{i,k}\cos(n\theta_k) + \sum_{k=1,k\neq k^*}^{\lfloor\frac{m}{2}\rfloor} D_{i,k}\sin(n\theta_k).
\end{aligned} \tag{38}
$$

Here $A_{i,k}$, $B_{i,k}$, $C_{i,k}$, $D_{i,k}$ are given from equation 31 for $\tilde{\omega} = \theta_{k^*} + 2l_1\pi$, $l_1 = 0, 1, 2, \ldots$, while

$$
\tilde{A}_{i,k^*} = -\frac{(a^*_{i,k^*}\cos\theta_{k^*} + b^*_{i,k^*})}{2\sin\theta_{k^*}}, \tilde{B}_{i,k^*} = \frac{a^*_{i,k^*}}{2}, \tilde{C}_{i,k^*} = \frac{a^*_{i,k^*} + b^*_{i,k^*}\cos\theta_{k^*}}{2\sin^2\theta_{k^*}}. \tag{39}
$$

As before, $b_{i,0} = 0$ for m even and $\sin\theta_k \neq 0$ for all $k = 1, \ldots, \lfloor\frac{m}{2}\rfloor$. The stress solutions in equation 38, including all the coefficients and angles θ_k for $k = 1, \ldots, \lfloor\frac{m}{2}\rfloor$, can be also expressed in terms of the impedance ratios only (see equations 6–9, equation 14, and appendices D and E).

All the terms in the stress solution in equation 38 are bounded, except for those that are multiplied by the time-related linear factor n given below

$$
\begin{aligned}
n\tilde{A}_{i,k^*}\cos(n\theta_{k^*}) + n\tilde{B}_{i,k^*}\sin(n\theta_{k^*}) &= -\frac{n}{2}\left[\frac{(a^*_{i,k^*}\cos\theta_{k^*} + b^*_{i,k^*})}{\sin\theta_{k^*}}\cos(n\theta_{k^*}) - a^*_{i,k^*}\sin(n\theta_{k^*})\right] \\
&= -\frac{n}{2}\left[\frac{a^*_{i,k^*}\cos\left[(n+1)\theta_{k^*}\right] + b^*_{i,k^*}\cos\left[(n\theta_{k^*})\right]}{\sin\theta_{k^*}}\right],
\end{aligned} \tag{40}
$$

where $a^*_{i,k^*} \neq 0$ or $b^*_{i,k^*} \neq 0$ for $i = 1, 2, \ldots, m$. This implies that the stress amplitude is expected to grow without bound over time, proving resonance for the frequency spectrum $\tilde{\omega}_{l_1,k^*} = \theta_{k^*} + 2l_1\pi$, $l_1 = 0, 1, 2, \ldots$, included in equation 15.

2.2.4 Case II.b.: $\sin\tilde{\omega} = -\sin\theta_{k^*} = \sin(-\theta_{k^*})$

A similar stress representation to equation 38 can be obtained at the frequency values $\tilde{\omega}_{l_2,k^*} = -\theta_{k^*} + 2(l_2+1)\pi$, $l_2 = 0, 1, 2, \ldots$, after a sign adjustment for some of the coefficients. The presence of resonance proves that this frequency spectrum is also part of the resonance frequency spectrum identified in equation 15.

In summary, we related to an m-layered Goupillaud-type strip with all the zeros of $|\mathbf{A_m}|$ on the unit circle, its corresponding set of angles $\theta_0 = \pi$ (for m odd only) and $\{\pm\theta_k\}_{k=1}^{\lfloor\frac{m}{2}\rfloor}$. In general,

the same set of angles could correspond to more than one layered design. When the strip was subjected to a harmonic forcing $f(n) = \sin(n\tilde{\omega})$ or $f(n) = \cos(n\tilde{\omega})$ at one end and held fixed at the other end, we showed that the positive angles coterminal with $\theta_0 = \pi$ (for m odd only) and $\{\pm\theta_k\}_{k=1}^{\lfloor \frac{m}{2} \rfloor}$ represented values of the driving frequency $\tilde{\omega}$, which produced resonance (see equation 15 or 16). The complement of this set of values in the set of real numbers was shown to represent the set of non-resonance frequencies.

In section 2.3 we demonstrate this approach and validate some of the results mainly for the two- and three-layer case. According to appendix B and equations D-1 and D-2 in appendix D, a Goupillaud-type strip with $m = 2, 3$ has all the zeros of $|\mathbf{A_m}|$ on the unit circle, hence a resonance spectrum given by equation 15. For simplicity, we continue to choose $f(n) = \sin(n\tilde{\omega})$, $n \geq 0$, unless mentioned otherwise.

2.3 The Two-layer Case ($m = 2$)

For the two-layer case, it follows from equations 21–22 that $\tilde{\omega} = \tau\omega$ and $f(n) = \sin(n \cdot \tau\omega) = \sin(n\tilde{\omega})$. As a result, equation 17 becomes

$$\tilde{\mathbf{x}}_\mathbf{2} = \frac{z\sin(\tilde{\omega})}{(z^2 - 2z\cos\tilde{\omega} + 1)} \cdot \begin{bmatrix} \frac{2z^2+2z}{\chi_1(z^2-2z\cos\theta_1+1)} \\ \\ \frac{4z^2}{\chi_1(z^2-2z\cos\theta_1+1)} \end{bmatrix}, \tag{41}$$

where $\chi_1 = 1 + \alpha_1 > 1$ and $\cos\theta_1 = \frac{\chi_1 - 2}{\chi_1} \neq \pm 1$ from equation D-1.

2.3.1 Stress Solutions at Non-resonance Frequencies

When $\cos\tilde{\omega} \neq \cos\theta_1$, we obtain the following bounded stress solutions

$$\begin{aligned} \begin{bmatrix} s_1(n) \\ \\ s_2(n) \end{bmatrix} &= Z^{-1}(\tilde{\mathbf{x}}_\mathbf{2}) \\ &= \frac{1}{\chi_1(\cos\tilde{\omega} - \cos\theta_1)} \begin{bmatrix} \sin\tilde{\omega}\cos(n\tilde{\omega}) + (1+\cos\tilde{\omega})\sin(n\tilde{\omega}) - \sin\tilde{\omega}\cos(n\theta_1) - \frac{(1+\cos\theta_1)\sin\tilde{\omega}}{\sin\theta_1}\sin(n\theta_1) \\ \\ 2\sin\tilde{\omega}\cos(n\tilde{\omega}) + 2\cos\tilde{\omega}\sin(n\tilde{\omega}) - 2\sin\tilde{\omega}\cos(n\theta_1) - \frac{2\cos\theta_1\sin\tilde{\omega}}{\sin\theta_1}\sin(n\theta_1) \end{bmatrix}, \end{aligned} \tag{42}$$

by applying equations 25 and 30 to equation 41. As the driving frequency $\tilde{\omega}$ approaches any of the values from the resonance frequency spectrum in equation 15, the denominator $(\cos\tilde{\omega} - \cos\theta_1)$ of the coefficients of the stress solutions gets close to zero, allowing the stress amplitude to take larger values.

Illustrations of the bounded stress solutions at non-resonance frequencies appear in figure 3. As depicted in the plots in figure 3 and discussed previously in this section, when positioned in the middle of the second layer, the time interval at which $s_i(n)$ is reached is $\frac{4n+2i-3}{4} < t < \frac{4n+2i-1}{4}$ for $n \geq 1$ and $i = 1, 2$ (see figure 1). Beat phenomena are clearly visible in figure 3(b), as the driving frequency approaches a resonance frequency.

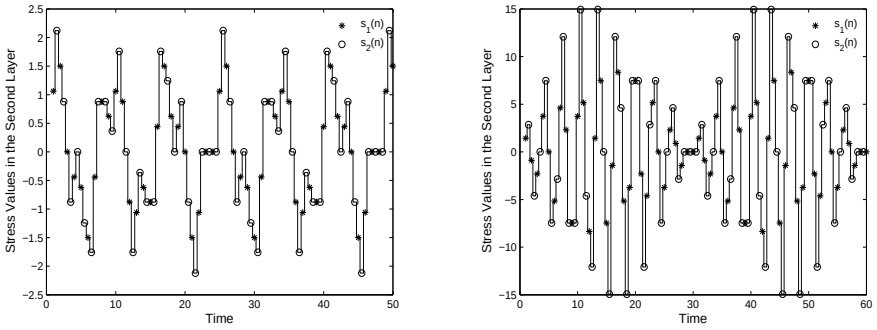

Figure 3. Stress time history for a two-layered Goupillaud-type strip in the middle of the second layer located at $\xi = 3/4$. Impedance ratio $\alpha_1 = 1/3$, angle $\theta_1 = 2\pi/3$, $\tau = 1$, and loading $f(n) = \sin(n\tilde{\omega})$ at $\xi = 0$. (a) $\tilde{\omega} = \pi/4$. (b) $\tilde{\omega} = 0.9 \cdot \theta_1 = 0.6\pi$.

2.3.2 Stress Solutions at Resonance Frequencies

When $\cos\tilde{\omega} = \cos\theta_1$ and $\sin\tilde{\omega} = \sin\theta_1$, the stress solutions become

$$\begin{bmatrix} s_1(n) \\ \\ s_2(n) \end{bmatrix} = \frac{1}{\chi_1} \begin{bmatrix} -\frac{(1+\cos\theta_1)}{\sin\theta_1} n\cos(n\theta_1) + \left[n + \frac{1}{1-\cos\theta_1} \right] \sin(n\theta_1) \\ \\ -\frac{2\cos\theta_1}{\sin\theta_1} n\cos(n\theta_1) + \left[2n + \frac{2}{\sin^2\theta_1} \right] \sin(n\theta_1) \end{bmatrix}, \tag{43}$$

by applying equations 25 and 38 to equation 41 for $\theta_{k^*} = \theta_1$. Further simplifications of equation 43 implies

$$\begin{aligned}
\begin{bmatrix} s_1(n) \\ \\ s_2(n) \end{bmatrix} &= -\frac{n}{\chi_1} \begin{bmatrix} \frac{\cos\left[\left(n+\frac{1}{2}\right)\theta_1\right]}{\sin\frac{\theta_1}{2}} \\ \\ \frac{2\cos[(n+1)\theta_1]}{\sin\theta_1} \end{bmatrix} + \frac{\sin(n\theta_1)}{\chi_1} \begin{bmatrix} \frac{1}{(1-\cos\theta_1)} \\ \\ \frac{2}{\sin^2\theta_1} \end{bmatrix} \\
&= -\begin{bmatrix} \frac{\cos\left[\left(n+\frac{1}{2}\right)\cos^{-1}\left(\frac{\chi_1-2}{\chi_1}\right)\right]}{\sqrt{\chi_1}} \\ \\ \frac{\cos\left[(n+1)\cos^{-1}\left(\frac{\chi_1-2}{\chi_1}\right)\right]}{\sqrt{\chi_1-1}} \end{bmatrix} \cdot n + \begin{bmatrix} \frac{1}{2} \\ \\ \frac{\chi_1}{2(\chi_1-1)} \end{bmatrix} \cdot \sin\left[n\cos^{-1}\left(\frac{\chi_1-2}{\chi_1}\right)\right].
\end{aligned} \tag{44}$$

Given that $0 < \theta_1 < \pi$, $\chi_1 = (1 + \alpha_1)$ and $\cos\theta_1 = \frac{\chi_1-1}{\chi_1}$, it follows that $\sin\theta_1 = \frac{2\sqrt{\chi_1-1}}{\chi_1}$ and $\sin\frac{\theta_1}{2} = \frac{1}{\sqrt{\chi_1}}$. Therefore, all the stress solutions can be expressed in terms of the design parameter χ_1 or equivalently in terms of the impedance ratio α_1 only, as shown in the last equality of equation 44.

As seen in figure 1, the stress values alternate between $f(n)$ and $s_1(n)$ in the first layer, and between $s_1(n)$ and $s_2(n)$ in the second layer, for $n = 1, 2, \ldots$. The terms of both stress sequences $s_1(n)$ and $s_2(n)$ become unbounded over time due to the (time-related) linear factor n (see equation 44). This implies that the stress amplitude will grow without bound in each layer, confirming resonance. Based on these results, we expect to detect resonance in both, the first and second layer, as illustrated in figure 4. The good agreement between the analytical results generated from equation 38, or equivalently equation 44, and the stress values generated from the recursive equations 2 for $s_1(n)$ and $s_2(n)$, $n \geq 1$, is displayed in figure 5. The fact that the linear factor n in equation 44 multiplies a cosine function explains the sinusoidal fluctuations of the stress solutions in figures 4–5.

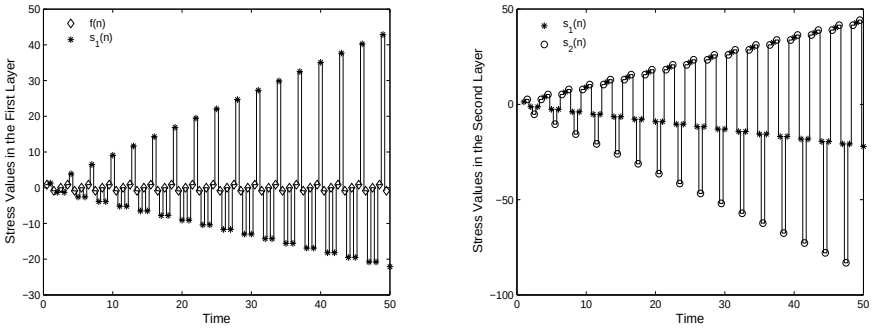

(a) (b)

Figure 4. Stress time history for a two-layered Goupillaud-type strip with impedance ratio $\alpha_1 = 1/3$, $\tau = 1$, subjected to loading $f(n) = \sin(n\tilde{\omega})$ with $\tilde{\omega} = \theta_1 = 2\pi/3$. (a) Middle of the first layer located at $\xi = 1/4$. (b) Middle of the second layer located at $\xi = 3/4$.

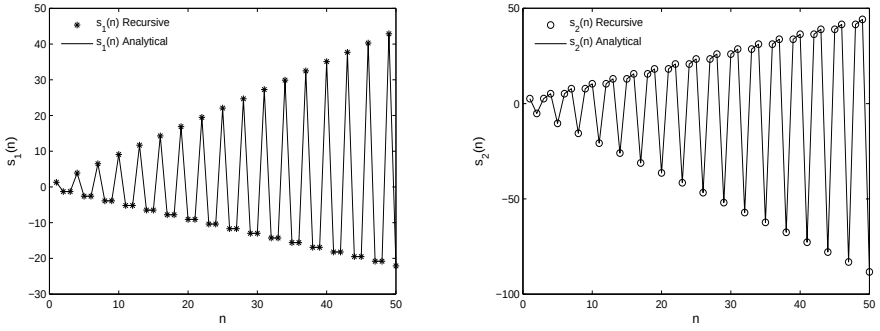

(a) (b)

Figure 5. The values of the two stress sequences (a) $s_1(n)$, (b) $s_2(n)$, obtained from the recursive equations 2 and the analytical equation 38, for the two-layered Goupillaud-type strip with impedance ratio $\alpha_1 = 1/3$, $\tau = 1$, subjected to loading $f(n) = \sin(n\tilde{\omega})$ with $\tilde{\omega} = \theta_1 = 2\pi/3$.

2.4 The Three-layer Case ($m = 3$)

For the three-layer case, it follows from equations 21–22 that $\tilde{\omega} = \frac{2\tau}{3}\omega$ and $f(n) = \sin(n \cdot \frac{2\tau}{3}\omega) = \sin(n\tilde{\omega})$. As a result, the first equation of 17 becomes

$$\tilde{\mathbf{x}}_{\mathbf{3}} = \frac{z^2 \sin(\tilde{\omega})}{(z^2 - 2z\cos\tilde{\omega} + 1)} \cdot \begin{bmatrix} \frac{2(1+\alpha_2)z^2+4(1-\alpha_2)z+2(1+\alpha_2)}{\chi_2(z+1)(z^2-2z\cos\theta_1+1)} \\ \\ \frac{4z}{\chi_2(z^2-2z\cos\theta_1+1)} \\ \\ \frac{8z^2}{\chi_2(z+1)(z^2-2z\cos\theta_1+1)} \end{bmatrix}, \tag{45}$$

where $\chi_2 = (1+\alpha_1)(1+\alpha_2) > 1$, $\cos\theta_0 = -1$, and $\cos\theta_1 = \frac{\chi_2 - 2}{\chi_2} \neq \pm 1$ from equation D-2 in appendix D. Applying in equation 45 partial fraction expansion as shown and equation 25, results in

$$\begin{bmatrix} s_1(n) \\ \\ s_2(n) \\ \\ s_3(n) \end{bmatrix} = Z^{-1}(\tilde{\mathbf{x}}_{\mathbf{3}}) = Z^{-1}\{\frac{1}{\chi_2} \cdot \frac{z^2\sin(\tilde{\omega})}{(z^2-2z\cos\tilde{\omega}+1)} \cdot \begin{bmatrix} \frac{2}{1+\cos\theta_1} \cdot \left[\frac{2\alpha_2}{z+1} + \frac{[(1+\alpha_2)\cos\theta_1+(1-\alpha_2)](z+1)}{z^2-2z\cos\theta_1+1} \right] \\ \\ \frac{4z}{z^2-2z\cos\theta_1+1} \\ \\ \frac{4}{1+\cos\theta_1} \cdot \left[\frac{1}{z+1} + \frac{(1+2\cos\theta_1)z-1}{z^2-2z\cos\theta_1+1} \right] \end{bmatrix}\}. \tag{46}$$

2.4.1 Stress Solutions at Non-resonance Frequencies

When $\cos\tilde{\omega} \neq -1 = \cos\theta_0$ and $\cos\tilde{\omega} \neq \cos\theta_1$, bounded stress solutions are obtained by applying equation 30 to equation 46 and further simplifying the results,

$$\begin{bmatrix} s_1(n) \\ s_2(n) \\ s_3(n) \end{bmatrix} = \frac{1}{\chi_2}\{ \begin{bmatrix} \frac{-2\alpha_2 \sin\tilde{\omega}}{(1+\cos\tilde{\omega})(1+\cos\theta_1)} \\ 0 \\ -\frac{2\sin\tilde{\omega}}{(1+\cos\tilde{\omega})(1+\cos\theta_1)} \end{bmatrix} (-1)^n + \begin{bmatrix} \frac{[(1+\alpha_2)\cos\tilde{\omega}+(1-\alpha_2)]\sin\tilde{\omega}}{(\cos\tilde{\omega}-\cos\theta_1)(1+\cos\tilde{\omega})} \\ \frac{2\sin\tilde{\omega}}{(\cos\tilde{\omega}-\cos\theta_1)} \\ \frac{2(2\cos\tilde{\omega}+1)\sin\tilde{\omega}}{(\cos\tilde{\omega}-\cos\theta_1)(1+\cos\tilde{\omega})} \end{bmatrix} \cos(n\tilde{\omega})$$

$$+ \begin{bmatrix} \frac{(1+\alpha_2)\cos\tilde{\omega}+(1-\alpha_2)}{(\cos\tilde{\omega}-\cos\theta_1)} \\ \frac{2\cos\tilde{\omega}}{(\cos\tilde{\omega}-\cos\theta_1)} \\ \frac{2(2\cos\tilde{\omega}-1)}{(\cos\tilde{\omega}-\cos\theta_1)} \end{bmatrix} \sin(n\tilde{\omega}) - \begin{bmatrix} \frac{[(1+\alpha_2)\cos\theta_1+(1-\alpha_2)]\sin\tilde{\omega}}{(\cos\tilde{\omega}-\cos\theta_1)(1+\cos\theta_1)} \\ \frac{2\sin\tilde{\omega}}{(\cos\tilde{\omega}-\cos\theta_1)} \\ \frac{2(2\cos\theta_1+1)\sin\tilde{\omega}}{(\cos\tilde{\omega}-\cos\theta_1)(1+\cos\theta_1)} \end{bmatrix} \cos(n\theta_1) \quad (47)$$

$$- \begin{bmatrix} \frac{[(1+\alpha_2)\cos\theta_1+(1-\alpha_2)]\sin\tilde{\omega}}{(\cos\tilde{\omega}-\cos\theta_1)\sin\theta_1} \\ \frac{2\cos\theta_1\sin\tilde{\omega}}{(\cos\tilde{\omega}-\cos\theta_1)\sin\theta_1} \\ \frac{2(2\cos\theta_1-1)\sin\tilde{\omega}}{(\cos\tilde{\omega}-\cos\theta_1)\sin\theta_1} \end{bmatrix} \sin(n\theta_1) \}.$$

As the driving frequency $\tilde{\omega}$ approaches any of the values from the resonance frequency spectrum in equation 15, the denominators $(\cos\tilde{\omega}+1)$ or $(\cos\tilde{\omega}-\cos\theta_1)$ of the coefficients of the stress solutions in equation 47 get close to zero, allowing the stress amplitude to take larger values.

Illustrations of the bounded stress solutions at non-resonance frequencies are given in figure 6. As depicted in figure 6 and discussed previously in this section, when positioned in the middle of the second or third layer, the time interval at which $s_i(n)$ is reached is $\frac{4n+2i-3}{6} < t < \frac{4n+2i-1}{6}$, as applicable, for $n \geq 1$ and $i = 1, 2, 3$ (see figure 1). The good agreement between the analytical results generated from equation 30, or equivalently equation 47, and the stress values generated from the recursive equations 2 for $s_1(n)$, $n \geq 1$, as well as the error introduced by the computational approximation of quantities (such as sine and cosine values), are displayed in figure 7.

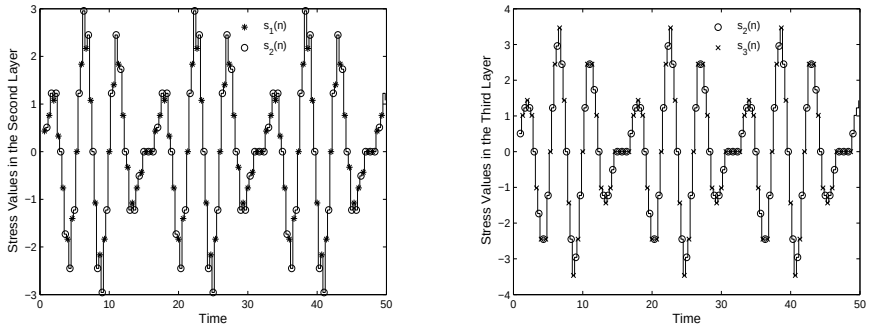

(a) (b)

Figure 6. Stress time history for a three-layered Goupillaud-type strip with $\alpha_1 = 3$, $\alpha_2 = \frac{1}{2(1-\cos(\pi/4))} - 1$, $\theta_1 = \frac{\pi}{4}$, $\tau = 1$, subjected to loading $f(n) = \sin(n\tilde{\omega})$ with $\tilde{\omega} = \frac{\pi}{3}$. (a) Middle of the second layer located at $\xi = 1/2$. (b) Middle of the third layer located at $\xi = 5/6$.

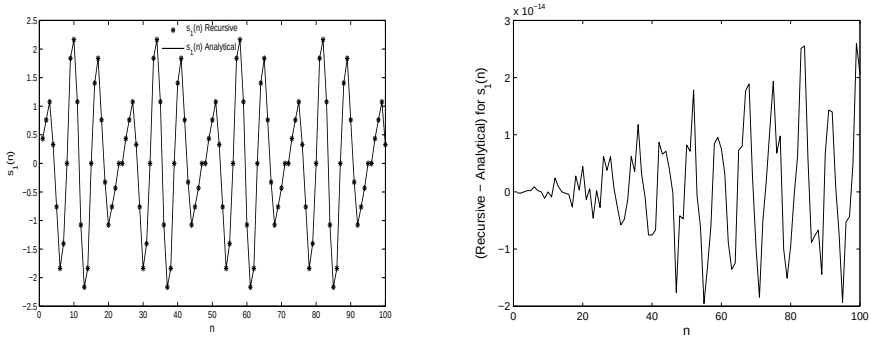

(a) (b)

Figure 7. The three-layered Goupillaud-type strip with $\alpha_1 = 3$, $\alpha_2 = \frac{1}{2(1-\cos(\pi/4))} - 1$, $\theta_1 = \frac{\pi}{4}$, $\tau = 1$, subjected to loading $f(n) = \sin(n\tilde{\omega})$ with $\tilde{\omega} = \frac{\pi}{3}$. (a) The values of the stress sequence $s_1(n)$, obtained from the recursive equations 2 and the analytical equation 30. (b) The difference of the expressions for $s_1(n)$ obtained from the recursive equations 2 and the analytical equation 30.

2.4.2 Stress Solutions at Resonance Frequencies

2.4.2.1 Case I. $\cos\tilde{\omega} = -1 = \cos\theta_0$

The stress formulas in the z-space for the three-layer case in equation 45, indicate that the sequences $s_1(n)$ and $s_3(n)$ increase without bound because $\cos(\tilde{\omega}) = -1 = \cos\theta_0$ corresponds to a zero of the denominator $z = e^{\mathcal{I}\theta_0} = -1$. Alternatively, we do not expect unbounded growth for the sequence $s_2(n)$, since $z = e^{\mathcal{I}\theta_0} = -1$ is not a zero of the denominator. Figure 8 illustrates this behavior for each of the stress sequences. Similar behavior was observed in the numerical experiments for the seven- and eleven-layer case (see illustration in figure 2) where the stress sequences with odd subindices increase without bound while the stress sequences with even subindices are bounded.

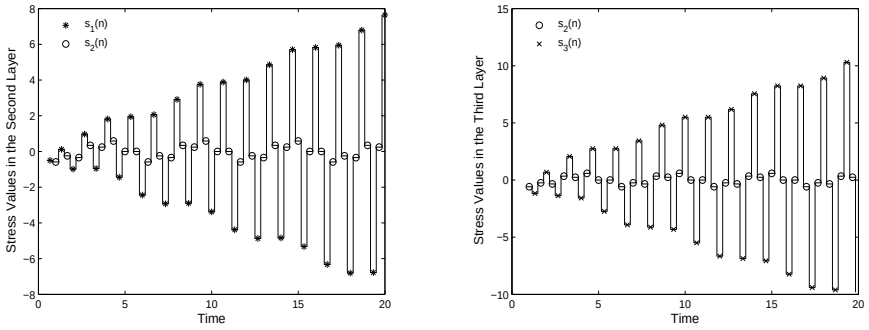

(a) (b)

Figure 8. Stress time history for a three-layered Goupillaud-type strip with $\alpha_1 = 3$, $\alpha_2 = \frac{1}{2(1-\cos(\pi/4))} - 1$, $\tau = 1$, subjected to loading $f(n) = \cos(n\tilde{\omega})$ with $\tilde{\omega} = \pi$. (a) Middle of the second layer located at $\xi = 1/2$. (b) Middle of the third layer located at $\xi = 5/6$.

2.4.2.2 Case II.a.

When $\cos\tilde{\omega} = \cos\theta_1$ and $\sin\tilde{\omega} = \sin\theta_1$, and by applying equation 38 to equation 46 the stress solutions become,

$$\begin{bmatrix} s_1(n) \\ s_2(n) \\ s_3(n) \end{bmatrix} = -\frac{2\sin\theta_1}{\chi_2(1+\cos\theta_1)^2}\begin{bmatrix} \alpha_2 \\ 0 \\ 1 \end{bmatrix}(-1)^n + \frac{2}{\chi_2}\begin{bmatrix} \frac{\alpha_2\sin\theta_1}{(1+\cos\theta_1)^2} - \frac{[(1+\alpha_2)\cos\theta_1+(1-\alpha_2)]}{2\sin\theta_1}n \\ -\frac{\cos\theta_1}{\sin\theta_1}n \\ \frac{\sin\theta_1}{(1+\cos\theta_1)^2} - \frac{(2\cos\theta_1-1)}{\sin\theta_1}n \end{bmatrix}\cos(n\theta_1)$$

$$+\frac{2}{\chi_2}\begin{bmatrix} \frac{(1-\alpha_2)\cos\theta_1+(1+\alpha_2)}{2\sin^2\theta_1} + \frac{[(1+\alpha_2)\cos\theta_1+(1-\alpha_2)]}{2(1+\cos\theta_1)}n \\ n + \frac{1}{\sin^2\theta_1} \\ \frac{2-\cos\theta_1}{\sin^2\theta_1} + \frac{(2\cos\theta_1+1)}{1+\cos\theta_1}n \end{bmatrix}\sin(n\theta_1). \tag{48}$$

Since the focus here is the study of resonance, the unbounded part of each of the stress solutions containing the time-related factor n can be simplified as follows:

$$\frac{2n}{\chi_2}\begin{bmatrix} -\frac{[(1+\alpha_2)\cos\theta_1+(1-\alpha_2)]}{2\sin\theta_1}\cos(n\theta_1) + \frac{[(1+\alpha_2)\cos\theta_1+(1-\alpha_2)]}{2(1+\cos\theta_1)}\sin(n\theta_1) \\ -\frac{\cos\theta_1}{\sin\theta_1}\cos(n\theta_1) + \sin(n\theta_1) \\ -\frac{(2\cos\theta_1-1)}{\sin\theta_1}\cos(n\theta_1) + \frac{(2\cos\theta_1+1)}{1+\cos\theta_1}\sin(n\theta_1) \end{bmatrix} =$$

$$-\frac{2n}{\chi_2}\begin{bmatrix} \frac{[(1+\alpha_2)\cos\theta_1+(1-\alpha_2)]}{2\cos\frac{\theta_1}{2}\sin\theta_1}\cos\left[\left(n+\frac{1}{2}\right)\theta_1\right] \\ \frac{\cos[(n+1)\theta_1]}{\sin\theta_1} \\ \frac{\cos\left[\left(n+\frac{3}{2}\right)\theta_1\right]}{\cos\frac{\theta_1}{2}\sin\theta_1} \end{bmatrix} = -n\begin{bmatrix} \frac{2\alpha_1\sqrt{\chi_2}}{(1+\alpha_1)(\chi_2-1)}\cos\left[\left(n+\frac{1}{2}\right)\cos^{-1}\frac{\chi_2-2}{\chi_2}\right] \\ \frac{\cos\left[(n+1)\cos^{-1}\frac{\chi_2-2}{\chi_2}\right]}{\sqrt{\chi_2-1}} \\ \frac{\sqrt{\chi_2}}{(\chi_2-1)}\cdot\cos\left[\left(n+\frac{3}{2}\right)\cos^{-1}\frac{\chi_2-2}{\chi_2}\right] \end{bmatrix} \tag{49}$$

Given that $0 < \theta_1 < \pi$, $\chi_2 = (1+\alpha_1)(1+\alpha_2)$, and $\cos\theta_1 = \frac{\chi_2-2}{\chi_2}$, it follows that $\sin\theta_1 = \frac{2\sqrt{\chi_2-1}}{\chi_2}$. Therefore, the stress solutions can be expressed in terms of the impedance ratios α_1 and α_2 only. This is demonstrated in the last equality (equation 49).

As seen in figure 1, the stress values alternate between $f(n)$ and $s_1(n)$ in the first layer, between $s_1(n)$ and $s_2(n)$ in the second layer, and between $s_2(n)$ and $s_3(n)$ in the third layer, for $n = 1, 2, \ldots$. All three stress sequences/solutions $s_1(n)$, $s_2(n)$, and $s_3(n)$ become unbounded over time due to the (time-related) linear factor n. This implies that the stress amplitude will grow without bound in all three layers (figure 9). The good agreement between the analytical results generated from equation 38, or equivalently equation 48, and the stress values generated from the recursive equations 2 for $s_1(n)$, $n \geq 1$, as well as the error introduced by the computational approximation of quantities (such as sine and cosine values) are displayed in figure 10. The fact that the linear factor n multiplies a cosine function as shown in equation 49, explains the sinusoidal fluctuations of the stress solutions in figures 9–10.

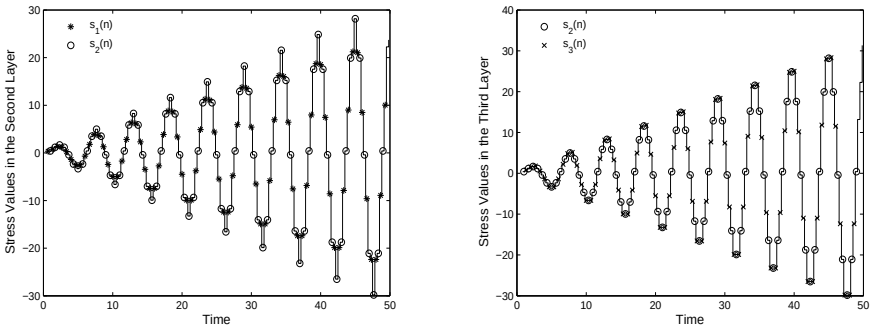

(a) (b)

Figure 9. Stress time history for a three-layered Goupillaud-type strip with $\alpha_1 = 3$, $\alpha_2 = \frac{1}{2(1-\cos(\pi/4))} - 1$, $\tau = 1$, subjected to loading $f(n) = \sin(n\tilde{\omega})$ with $\tilde{\omega} = \theta_1 = \frac{\pi}{4}$. (a) Middle of the second layer located at $\xi = 1/2$. (b) Middle of the third layer located at $\xi = 5/6$.

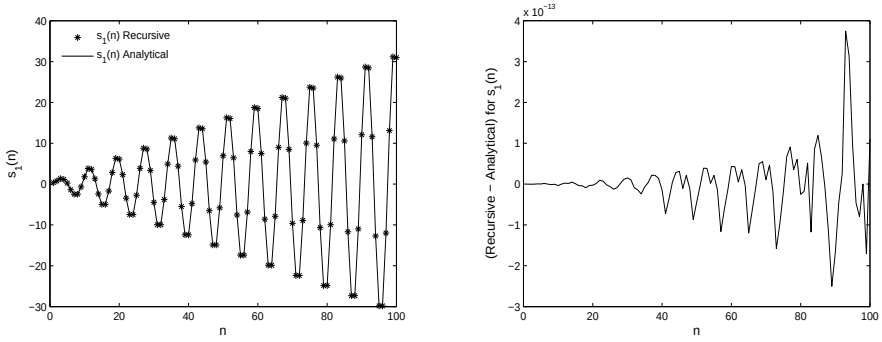

(a) (b)

Figure 10. (a) The values of the stress sequence $s_1(n)$, obtained from the recursive equations 2 and the analytical equation 38. (b) The difference of the expressions for $s_1(n)$ obtained from the recursive equations 2 and the analytical equation 38 for a three-layered Goupillaud-type strip with $\alpha_1 = 3$, $\alpha_2 = \frac{2}{2(1-\cos(\pi/4))} - 1$, $\tau = 1$, subjected to loading $f(n) = \sin(n\tilde{\omega})$ with $\tilde{\omega} = \theta_1 = \frac{\pi}{4}$.

3. Analytical Formulas for the Natural Frequency Spectrum of a Free-fixed Goupillaud-type Layered Elastic Strip

In this section, we derive the natural frequencies of a free-fixed m-layered Goupillaud-type strip in two different ways:

1. By simplifying and then solving the frequency equation for $2 \leq m \leq 5$.
2. By extending the results of the resonance frequency spectrum from the discrete model to the continuous model for any $m \geq 2$. In the continuous model, the strip is subjected to a continuous harmonic forcing function at one end and held fixed at the other end.

3.1 The Frequency Equation: Explicit Formula for the Natural Frequency Spectrum

The frequency equation for a free-fixed m-layered Goupillaud-type strip is derived in this section, by generalizing the procedure described in Graff (*33*). The frequency equation is simplified through a transformation of the spatial variable, to derive the natural frequency spectrum for $2 \leq m \leq 5$.

The governing equations for the displacement $u(x,t)$ in each layer of the strip are:

$$\frac{\partial^2 u_i(x,t)}{\partial t^2} = c_i^2 \frac{\partial^2 u_i(x,t)}{\partial x^2} \quad \text{for } x_{i-1} < x < x_i, \quad i = 1, \ldots, m, \tag{50}$$

where $0 = x_0 < x_1 < \cdots x_i < \cdots < x_m = L$, L represents the length of the strip, c_i represents the wave speed in the ith layer, x represents the spatial variable, and $t \geq 0$ represents the time variable. Seeking harmonic solutions, we may represent $u(x,t) = U(x)\psi(t)$ and the spatial component(s) of the displacement for each layer as

$$U_i(x) = A_i \sin \beta_i x + B_i \cos \beta_i x \quad \text{for } x_{i-1} < x < x_i, \quad i = 1, \ldots, m, \tag{51}$$

where $\beta_i = \omega / c_i$ for $i = 1, \ldots, m$, and ω represents the frequency of the harmonic motion. Similarly, $\psi(t)$ can be represented in the form $\psi(t) = A^* \sin \omega t + B^* \cos \omega t$ or in exponential form as $\psi(t) = A^{**} e^{\mathcal{I}\omega t} + B^{**} e^{-\mathcal{I}\omega t}$, where $\mathcal{I} = \sqrt{-1}$. As a result, after applying the free-fixed boundary conditions at $x = 0$ and $x = L$, respectively,

$$\frac{dU_1(0)}{dx} = U_m(L) = 0, \tag{52}$$

and the continuity of stress and displacement at each layer interface, results in the following linear system of equations:

$$\begin{cases} A_1 = 0, & \\ A_i \sin\left(\frac{\omega}{c_i} x_i\right) + B_i \cos\left(\frac{\omega}{c_i} x_i\right) = A_{i+1} \sin\left(\frac{\omega}{c_{i+1}} x_i\right) + B_{i+1} \cos\left(\frac{\omega}{c_{i+1}} x_i\right) & \text{for } i = 1, \ldots, m-1, \\ \alpha_i \left[A_i \cos\left(\frac{\omega}{c_i} x_i\right) - B_i \sin\left(\frac{\omega}{c_i} x_i\right)\right] = A_{i+1} \cos\left(\frac{\omega}{c_{i+1}} x_i\right) - B_{i+1} \sin\left(\frac{\omega}{c_{i+1}} x_i\right) & \text{for } i = 1, \ldots, m-1, \\ A_m \sin\left(\frac{\omega}{c_m} x_m\right) + B_m \cos\left(\frac{\omega}{c_m} x_m\right) = 0, & \end{cases} \tag{53}$$

The relations $\alpha_i = \frac{c_i \rho_i}{c_{i+1} \rho_{i+1}} = \frac{E_i}{c_i} \cdot \frac{c_{i+1}}{E_{i+1}}$ were applied equation 53, using the fact that $c \cdot \rho = E/c$. The condition that the determinant of the system matrix for equation 53 must vanish generates the frequency equation for ω. Solving the frequency equation and obtaining a general formula could be a challenging task. However, if the spatial variable x of the wave equation is replaced with the new variable $\xi = \int_0^x \frac{ds}{c(s)}$, the frequency equation can be simplified. This transformation converts the problem to a Goupillaud-type layered strip with the same length L as the wave transit time τ through the strip ($L = \tau$) (see Velo and Gazonas (*40*) and section 2). Under this transformation, the layers have equal lengths of $\frac{\tau}{m}$ and wave speed of unity. In addition, the previous coordinates $x_0 = 0$, x_j, and $x_m = L$ are replaced by the new coordinates $\xi_0 = 0$, $\xi_j = \frac{j\tau}{m}$, and $\xi_m = \tau$ for

$j = 1, 2, \ldots, m$, while the impedance ratio $\alpha_i = \frac{\tilde{E}_i}{\tilde{E}_{i+1}} = \frac{\sqrt{E_i \rho_i}}{\sqrt{E_{i+1} \rho_{i+1}}}$ remains the same for $i = 1, 2, \ldots, m-1$. As before, E_i, ρ_i represent the actual material properties for the physical case, while $\tilde{E}_i$, $\tilde{\rho}_i$ represent the material properties of the ith layer for the simplified case, with $\tilde{E}_i = \tilde{\rho}_i = \sqrt{E_i \rho_i}$. As seen next, both designs of the strip share the same natural frequency spectrum under free-fixed boundary conditions.

As a result, equation 53 can be transformed in a new matrix-vector form as follows:

$$\mathbf{\Delta_m} \tilde{\mathbf{v}} = \tilde{\mathbf{0}}, \tag{54}$$

where

$$\mathbf{\Delta_m} = \begin{bmatrix} 1 & 0 & 0 & 0 & \ldots & 0 \\ \sin\gamma_1 & & & & & \\ \alpha_1 \cos\gamma_1 & & & & & \\ 0 & & & & & \\ 0 & & & & & \\ \vdots & & & \tilde{\mathbf{\Delta}}_\mathbf{m} & & \\ & & & & & \\ & & & & & \\ & & & & & \\ 0 & & & & & \end{bmatrix}_{2m \times 2m}, \tilde{\mathbf{v}} = \begin{bmatrix} A_1 \\ B_1 \\ \vdots \\ A_i \\ B_i \\ \vdots \\ A_m \\ B_m \end{bmatrix}_{2m \times 1}, \tag{55}$$

and

$$\tilde{\mathbf{\Delta}}_\mathbf{m} = \begin{bmatrix} \cos\gamma_1 & -\sin\gamma_1 & -\cos\gamma_1 & 0 & 0 & 0 & 0 \\ -\alpha_1 \sin\gamma_1 & -\cos\gamma_1 & \sin\gamma_1 & 0 & & & \\ 0 & \sin\gamma_2 & \cos\gamma_2 & -\sin\gamma_2 & -\cos\gamma_2 & & \\ 0 & \alpha_2 \cos\gamma_2 & -\alpha_2 \sin\gamma_2 & -\cos\gamma_2 & \sin\gamma_2 & & \\ & \ddots & \ddots & \ddots & \ddots & \vdots & \vdots \\ 0 & \ldots & & & & 0 & 0 \\ 0 & \ldots & 0 & \sin\gamma_{m-1} & \cos\gamma_{m-1} & -\sin\gamma_{m-1} & -\cos\gamma_{m-1} \\ 0 & \ldots & 0 & \alpha_{m-1}\cos\gamma_{m-1} & -\alpha_{m-1}\sin\gamma_{m-1} & -\cos\gamma_{m-1} & \sin\gamma_{m-1} \\ 0 & \ldots & 0 & 0 & 0 & \sin\gamma_m & \cos\gamma_m \end{bmatrix}. \tag{56}$$

Here $\gamma_i = \xi_i \omega = \frac{i\tau\omega}{m}$ for $i = 1, \ldots, m$. Seeking a nonzero solution for equation 54, the determinant of the system matrix $\mathbf{\Delta_m}$ must vanish:

$$|\mathbf{\Delta_m}| = 0. \tag{57}$$

Equation 57 gives the transformed/simplified frequency equation for ω. Equation 57 can be successfully solved, using symbolic algebra software, for a strip with up to five layers (see appendix F). Solving the frequency equation 57 for the general m-layer case, poses a computational challenge.

Based on these derivations, a comparison of equation 14 with equation 57, equation D-1 with equation F-1, equation D-2 with equation F-3, equation D-4 with equation F-5, and equation D-6 with equation F-9 reveals that the two matrices $\mathbf{D_m}$ and $\mathbf{\Delta_m}$, defined in equation C-1 and equations 55–56, have the same dimensions and cosine roots of their determinants subject to the transformation

$$\cos\theta = \cos\frac{2\tau}{m}\omega. \tag{58}$$

Also notice that the pairs of the frequency equations F-1, F-3 and F-5, F-9, have a similar pattern to equations D-1, D-2 and D-4, D-6, respectively. Equations 58 can be justified from equations 21–22 and the fact that the natural frequencies of a free-fixed elastic strip correspond to the resonance frequencies when a (continuous) forcing, which varies harmonically with time is applied at the free end of the strip.

3.2 Heuristic Approach: Implicit General Formula for the Natural Frequency Spectrum

Using the linear frequency transformation in equation 21, the resonance frequency spectrum for the continuous model (where the strip is subjected to a continuous harmonic forcing at one end and held fixed at the other end) can be recovered from the resonance frequency results in equation 15 for the discrete model. This results in the following implicit formula for the natural frequency spectrum of a free-fixed m-layered Goupillaud-type strip:

$$\begin{cases} \omega_{l_0} = \frac{m}{2\tau}\cdot[\theta_0 + 2l_0\pi] = \frac{1}{2\left(\frac{\tau}{m}\right)}\cdot(2l_0+1)\pi, & \text{(for } m \text{ odd only)}, \\ \omega_{l_1,k} = \frac{m}{2\tau}\cdot[\theta_k + 2l_1\pi] = \frac{1}{2\left(\frac{\tau}{m}\right)}\cdot[\theta_k + 2l_1\pi], & l_0, l_1, l_2 = 0, 1, 2, \ldots, \\ \omega_{l_2,k} = \frac{m}{2\tau}\cdot[-\theta_k + 2(l_2+1)\pi] = \frac{1}{2\left(\frac{\tau}{m}\right)}\cdot[-\theta_k + 2(l_2+1)\pi], & k = 1, \ldots, \lfloor\frac{m}{2}\rfloor. \end{cases} \tag{59}$$

Substitution of the angle values from equations D-1, D-3, D-5, and D-7 into equation 59, results in the natural frequency spectrum for the free-fixed Goupillaud-type layered strip with up to five layers, equations F-2, F-4, and F-6, derived independently in appendix F from the frequency equation 57. Although a rigorous proof for the equation 59 is not provided, our theoretical and numerical results validate it as the general natural frequency spectrum of a free-fixed m-layered Goupillaud-type strip with the zeros of the corresponding matrix $|\mathbf{A_m}|$ on the unit circle (see matrix $\mathbf{A_m}$ defined in the z-space in equation 7). The zeros of $|\mathbf{A_m}|$ on the unit circle generate the respective angles $\theta_0 = \pi$ (for m odd only) and $\{\pm\theta_k\}_{k=1}^{\lfloor \frac{m}{2} \rfloor}$ needed to recover the natural frequency spectrum.

3.3 Interpretation and Illustration of the Natural Frequency Results

The explicit natural frequency equations (F-2, F-4, and F-6) derived from the frequency equation 57, as well as the general frequency spectrum derived from the implicit equation 59, suggest that for a free-fixed m-layered Goupillaud-type strip, the natural frequency spectrum does not depend on the actual length of the strip. According to these formulas, the natural frequency spectrum depends only on certain combinations of the impedance ratios $\alpha_1, \alpha_2, \ldots, \alpha_{m-1}$ and (it is inversely proportional to) the (equal) wave travel time $\frac{\tau}{m}$ for each layer.

The following illustration validates these expectations and demonstrates the simplicity of predicting the natural frequency spectrum when using the general equation 59, or solving the simplified frequency equation 57, versus solving directly the frequency equation generated from equation 53. Our numerical experiments with up to five layers have shown that the natural frequency spectrum can be predicted using either equation 59 and appendix D, or appendix F, even when a symbolic algebra software such as Maple cannot solve the frequency equation obtained from equation 53.

3.3.1 Case a. Two-layered Goupillaud-type Elastic Strip with Unequal Layer Lengths

- Layer lengths: $L_1 = \sqrt{2}, L_2 = 3\sqrt{2}$
- Length of the strip: $L = L_1 + L_2 = 4\sqrt{2}$
- Wave speed per layer: $c_1 = 1, c_2 = 3$
- Elastic modulus per layer: $E_1 = 2 + \sqrt{3}, E_2 = 3(2 - \sqrt{3})$
- Wave travel time per layer: $\frac{L_1}{c_1} = \frac{L_2}{c_2} = \frac{\tau}{m} = \sqrt{2}$
- Transit time through the strip: $\tau = 2\sqrt{2}$
- Impedance ratio: $\alpha_1 = \frac{E_1}{c_1} \cdot \frac{c_2}{E_2} = \frac{2+\sqrt{3}}{2-\sqrt{3}}$

• Frequency equation from equation 53:

$$\begin{vmatrix} 1 & 0 & 0 & 0 \\ \sin\left(\sqrt{2}\,\omega\right) & \cos\left(\sqrt{2}\,\omega\right) & -\sin\left(\frac{\sqrt{2}}{3}\,\omega\right) & -\cos\left(\frac{\sqrt{2}}{3}\,\omega\right) \\ \alpha_1\cos\left(\sqrt{2}\,\omega\right) & -\alpha_1\sin\left(\sqrt{2}\,\omega\right) & -\cos\left(\frac{\sqrt{2}}{3}\,\omega\right) & \sin\left(\frac{\sqrt{2}}{3}\,\omega\right) \\ 0 & 0 & \sin\left(\frac{4\sqrt{2}}{3}\,\omega\right) & \cos\left(\frac{4\sqrt{2}}{3}\,\omega\right) \end{vmatrix} = 0. \tag{60}$$

3.3.2 Case b. Simplified Two-layered Goupillaud-type Elastic Strip with Equal Layer Lengths

This free-fixed strip has the same natural frequency spectrum as the one in Case a.

• Layer lengths: $\tilde{L}_1 = \frac{L_1}{c_1} = \tilde{L}_2 = \frac{L_2}{c_2} = \frac{\tau}{2} = \sqrt{2}$

• Length of the strip: $\tilde{L} = \tilde{L}_1 + \tilde{L}_2 = \tau = 2\sqrt{2}$

• Wave speed per layer: $\tilde{c}_1 = \tilde{c}_2 = 1$

• Elastic modulus per layer: $\tilde{E}_1 = 2 + \sqrt{3}, \tilde{E}_2 = 2 - \sqrt{3}$

• Wave travel time per layer: $\frac{\tilde{L}_1}{\tilde{c}_1} = \frac{\tilde{L}_2}{\tilde{c}_2} = \frac{\tau}{2} = \sqrt{2}$

• Transit time through the strip: $\tau = 2\sqrt{2}$

• Impedance ratio: $\tilde{\alpha}_1 = \frac{\tilde{E}_1}{\tilde{E}_2} = \frac{2+\sqrt{3}}{2-\sqrt{3}} = \alpha_1$

• Frequency equation from equation 57:

$$\begin{vmatrix} 1 & 0 & 0 & 0 \\ \sin\left(\sqrt{2}\,\omega\right) & \cos\left(\sqrt{2}\,\omega\right) & -\sin\left(\sqrt{2}\ \omega\right) & -\cos\left(\sqrt{2}\,\omega\right) \\ \alpha_1\cos\left(\sqrt{2}\,\omega\right) & -\alpha_1\sin\left(\sqrt{2}\,\omega\right) & -\cos\left(\sqrt{2}\,\omega\right) & \sin\left(\sqrt{2}\,\omega\right) \\ 0 & 0 & \sin\left(2\sqrt{2}\,\omega\right) & \cos\left(2\sqrt{2}\,\omega\right) \end{vmatrix} = 0. \tag{61}$$

3.3.3 The Predicted Natural Frequency Spectrum

The common natural frequency spectrum for the free-fixed strip, for Cases a. and b.:

$$\begin{cases} \omega_{l_1} = \frac{1}{2\sqrt{2}}\left(\frac{\pi}{6} + 2l_1\pi\right) = \frac{\pi}{12\sqrt{2}} + \frac{\pi}{\sqrt{2}}l_1, \\ \qquad\qquad\qquad\qquad\qquad\qquad\qquad\qquad l_1, l_2 = 0, 1, 2, \ldots, \\ \omega_{l_2} = \frac{1}{2\sqrt{2}}\left(-\frac{\pi}{6} + 2(l_2+1)\pi\right) = \frac{11\pi}{12\sqrt{2}} + \frac{\pi}{\sqrt{2}}l_2, \end{cases} \tag{62}$$

can be derived easily and accurately from equation 59 and equation D-1 for $\theta_1 = \cos^{-1}\left(\frac{\alpha_1 - 1}{\alpha_1 + 1}\right) = \frac{\pi}{6}$, or equation F-2. The Maple software recovers most of these results by finding the zeros of the determinants previously given in Cases a. and b. As expected, the frequency equation in the (simplified) Case b. is much easier to solve in Maple than the original frequency equation in Case a.

3.3.4 Case c. Design Modification That Gives a Desired Frequency Spectrum Within Limitations

One way to modify the natural frequency spectrum equation 62 is to modify any of the two layered strips given in Cases a. and b., with $\chi_1 = (1 + \alpha_1)$ and $\theta_1 = \frac{\pi}{6}$, by adding a new layer in front of the existing two layers. The length of the new layer must be chosen so that the strip remains of Goupillaud-type. The new three-layered strip is characterized by $\chi_2 = (1 + \alpha_1^*)(1 + \alpha_2^*)$ with α_1^* to be determined and $\alpha_2^* = \alpha_1$. For a desirable value of the cosine of the base angle θ_1^* given by $V = \cos\theta_1^* = \frac{\chi_2 - 2}{\chi_2}$, one can derive the necessary formula for the unknown impedance ratio α_1^*:

$$\alpha_1^* = -1 + \frac{2}{\chi_1(1 - V)}, \text{ where } \frac{\chi_1 - 2}{\chi_1} = \cos\theta_1 < V = \cos\theta_1^* < 1, \tag{63}$$

using the fact that $\chi_2 = (1 + \alpha_1^*)\chi_1$. For instance, for the choice of $\theta_1^* = \frac{\pi}{9}$ we have that $\cos\theta_1 = \cos\left(\frac{\pi}{6}\right) < V = \cos\theta_1^* = \cos\left(\frac{\pi}{9}\right)$, which results in the natural frequency spectrum:

$$\begin{cases} \omega_{l_0} = \frac{1}{2\sqrt{2}}\left(\pi + 2l_0\pi\right) = \frac{\pi}{2\sqrt{2}} + \frac{\pi}{\sqrt{2}}l_0, \\ \\ \omega_{l_1} = \frac{1}{2\sqrt{2}}\left(\frac{\pi}{9} + 2l_1\pi\right) = \frac{\pi}{18\sqrt{2}} + \frac{\pi}{\sqrt{2}}l_1, \qquad\qquad l_0, l_1, l_2 = 0, 1, 2, \ldots, \\ \\ \omega_{l_2} = \frac{1}{2\sqrt{2}}\left(-\frac{\pi}{9} + 2(l_2 + 1)\pi\right) = \frac{17\pi}{18\sqrt{2}} + \frac{\pi}{\sqrt{2}}l_2, \end{cases} \tag{64}$$

for the free-fixed three-layered strip with impedance ratios $\alpha_1^* = -1 + \frac{2 - \sqrt{3}}{2\left(1 - \cos\left(\frac{\pi}{9}\right)\right)}$, $\alpha_2^* = \frac{2 + \sqrt{3}}{2 - \sqrt{3}}$ and the (equal) wave travel time per layer $\frac{\tau^*}{3} = \frac{\tau}{2} = \sqrt{2}$.

4. Other Applications of the Frequency Results

The properties of the materials used in this section appear in appendix G. Using the definition of the wave speed $c = \sqrt{E/\rho}$, the characteristic impedance ρc in each layer is calculated in terms of the material properties as $\sqrt{E\rho}$. Once the length of one layer is chosen, the length of each remaining layer is determined according to the material properties to provide equal wave travel time: $\frac{L_i}{c_i} = \frac{L_{i+1}}{c_{i+1}}$ or $L_{i+1} = \sqrt{\frac{E_{i+1}}{\rho_{i+1}} \cdot \frac{\rho_i}{E_i}}\, L_i$. Here L_j, c_j, E_j and ρ_j, for $j = i, i+1$, represent the length, wave speed, elastic modulus, and material density for the ith and $(i+1)$th layer, respectively, $i = 1, \ldots, m-1$.

4.1 One-dimensional Layered Media with a Common Frequency Spectrum

According to equations 14 and 15, the resonance frequency spectrum for the discrete model depends only on certain combinations of the impedance ratios $\alpha_1, \alpha_2, \ldots, \alpha_{m-1}$. Such combinations of impedance ratios when $2 \leq m \leq 5$ are represented by the design parameters χ_{m-1} for $m = 2, 3$, and χ_{m-1}, Γ_{m-1} for $m = 4, 5$. There are (theoretically) infinitely many m-layered designs of a Goupillaud-type elastic strip, which have the same values of the design parameters χ_{m-1}, Γ_{m-1} for $2 \leq m \leq 5$, hence the same resonance frequency spectrum for the discrete model.

As for the natural frequency spectrum of a free-fixed m-layered Goupillaud-type strip based on equation 59, it depends not only on combinations of the impedance ratios $\alpha_1, \alpha_2, \ldots, \alpha_{m-1}$ but also on the (equal) wave travel time $\frac{\tau}{m}$ for each layer. Therefore, to obtain designs with a common natural frequency spectrum, besides having the same values of the relevant design parameters, the layer lengths have to be chosen so that they all have the same wave travel time. Another way to find designs with a common natural frequency spectrum was previously illustrated in subsection 3.3 using a transformation of the spatial variable.

For the three-layer case where $\chi_2 = (1+\alpha_1)(1+\alpha_2)$, the tungsten-lead-aluminum configuration with $\alpha_1 \approx 5.828$ and $\alpha_2 \approx 0.952$ has the same value of $\chi_2 \approx 13.33$ as the lead-aluminum-copper configuration with $\alpha_1 \approx 0.952$ and $\alpha_2 \approx 5.828$. Another material design with $\chi_2 \approx 13.33$ is the aluminum-steel-brass configuration with $\alpha_1 \approx 0.331$ and $\alpha_2 \approx 9.016$. In addition, in order for these material designs to have a common natural frequency spectrum for the free-fixed strip, only the length of one layer in one of the designs may be chosen at random. The lengths of the remaining layers in all the three designs are then determined to provide equal wave travel time.

For the four-layer case, we have that $\chi_3 = (1+\alpha_1)(1+\alpha_2)(1+\alpha_3)$ and $\Gamma_3 = \alpha_1\alpha_3 - 1$. The aluminum-(glass fiber reinforced material)-nickel-bronze configuration with $\alpha_1 \approx 2.27$, $\alpha_2 \approx 0.698$ and $\alpha_3 = 1/\alpha_1 \approx .44$, has almost the same value of $\chi_3 = 8$ and $\Gamma_3 = 0$, as the homogeneous strip (all "four layers" are made of the same elastic material). As a result, these designs share the same resonance frequency spectrum when subjected to a discrete harmonic forcing at one end and held fixed at the other end. The common frequency spectrum can be derived from equation 15 after substituting $\chi_3 = 8$ and $\Gamma_3 = 0$ into equation D-5. In addition, a common wave travel time for each of the four layers in both designs would ensure the same natural frequency spectrum under free-fixed boundary conditions.

Furthermore, according to equation D-5 and table E-1, these designs with parameters $\chi_3 = 8$ and $\Gamma_3 = 0$, and base angle values $\theta_{1,opt} = \pi/4$ and $\theta_{2,opt} = 3\pi/4$ obtained for $j = 2$, are expected to be optimal, i.e., provide a stress amplitude of double the loading when a Heaviside step in stress loading is applied at one end of the strip while the other end is held fixed.

4.2 Resonance Frequencies and Optimal Designs

For the m-layered strip subjected to a Heaviside loading (*40*), it was shown that when the optimal values of the base angles $\theta_{k,opt}$ for $k = 1, \ldots, \lfloor \frac{m}{2} \rfloor$, given in appendix E, were substituted into the respective angle-design parameter equations in appendix D, optimal m-layered designs were generated for $2 \leq m \leq 5$. These optimal designs provide the smallest stress amplitude of double the loading in all layers, for all times.

However, when these optimal angle values are substituted into equations 15 and 59, they generate the resonance frequency spectrum for the discrete and continuous model, respectively. This means that for the optimal designs identified in appendices D–E, the displacement and stress amplitude will grow without bound over time when a harmonic forcing with a resonance frequency is applied instead of the Heaviside loading. As a result, for these designs, depending on the type of loading, one can get either the best or the worst outcome when it comes to controlling the stress amplitude (see the illustration in figure 11). As previously seen in figure 1, the stress values in a two-layered strip are given by the sequences $f(n)$, $s_1(n)$, and $s_2(n)$, $n \geq 0$. For the example considered in figure 11(a), we have that $|f(n)| \leq 1$ for all $n \geq 0$, therefore the stress amplitude, which exceeds unity, is determined by the other two stress sequences. Similarly, for the example considered in figure 11(b) we have that $f(n) = 1$ for all $n \geq 0$, therefore the stress amplitude, which exceeds unity, is also determined by the other two stress sequences. Notice that as the stress amplitude in figure 11(a) grows without bound over time for a harmonic forcing condition, the stress amplitude in figure 11(b) does not exceed double the

loading for a Heaviside loading condition. Examples of such material designs were given in the previous subsection for the four-layer case.

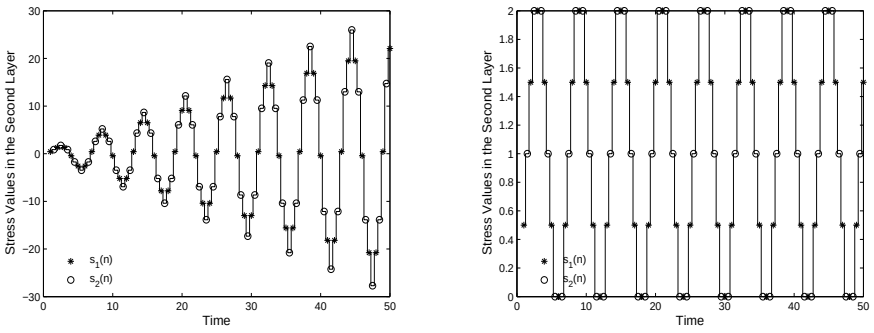

(a) (b)

Figure 11. Stress time history for a two-layered Goupillaud-type strip with impedance ratio $\alpha_1 = 3$, $\theta_1 = \frac{\pi}{3}$, $\tau = 1$, at the middle of the second layer located at $\xi = 3/4$ subjected to loading (a) $f(n) = \sin(n\tilde{\omega})$ with $\tilde{\omega} = \theta = \frac{\pi}{3}$. (b) $f(n) = 1$ for $n \geq 0$.

4.3 Natural Frequencies of a Free-fixed Non-Goupillaud-type Layered Strip with Integer Layer Length Ratios

The natural frequency results for a free-fixed Goupillaud-type layered strip with equal layer lengths given in equations F-1 through F-9, may be extended to a free-fixed non-Goupillaud-type layered strip with integer layer length ratios. We illustrate this with the two examples included below.

A three-layered Goupillaud-type strip with equal layer lengths ($\alpha_2 = 1$ or $\alpha_1 = 1$), represents a two-layered non-Goupillaud-type strip with 1:2 or 2:1 wave travel time ratios respectively. The case with 1:2 ratio requires that $\alpha_2 = 1$ and equation F-3 becomes

$$\cos\frac{2\tau}{3}\omega = -1 \text{ or } \cos\frac{2\tau}{3}\omega = \frac{\alpha_1}{1+\alpha_1}, \text{ for } \alpha_1 > 0. \tag{65}$$

Similar results to equation 65 can be obtained for the case with 2:1 ratio which requires that $\alpha_1 = 1$.

The frequency results for a free-fixed four-layered Goupillaud-type strip with equal layer lengths given in equation F-5, can be extended to a free-fixed three-layered non-Goupillaud-type strip with wave travel time ratios 1:2:1 by choosing $\alpha_2 = 1$. With these conditions, equation F-5

becomes

$$(1+\alpha_1)(1+\alpha_3)\cos^2\frac{\tau}{2}\omega - \Gamma_3\cos\frac{\tau}{2}\omega + (\Gamma_3 - (1+\alpha_1)(1+\alpha_3) + 2) = 0, \tag{66}$$

where $\Gamma_3 = (\alpha_1\alpha_3 - 1)$ is chosen so that the (cosine) solutions vary in the interval $[-1, 1]$. This can be achieved when $\Gamma_3 = 0$, which implies that $(1+\alpha_1)(1+\alpha_3) > 2$. As a result, equation 66 reduces to:

$$0 < \cos^2\left(\frac{\tau}{2}\omega\right) = \frac{(1+\alpha_1)(1+\alpha_3) - 2}{(1+\alpha_1)(1+\alpha_3)} < 1. \tag{67}$$

4.4 Representation of the Stress Solutions in Terms of the Chebyshev Polynomials

The formulas related to the stress solutions in equations 30, 35, and 38 consist of sums with terms of the form $\cos(n\phi)$, $\sin(n\phi)$, $(-1)^n$, n and $(-1)^n(n+1)$. These terms relate to the Chebyshev polynomials of the first and second kind $T_n(y)$ and $W_n(y)$, respectively (see Schaum (*44*)), as shown below:

$$\cos(n\phi) = T_n(\cos\phi),\ (-1)^n = T_n(-1),\ n = W_n(1) - 1,\ (-1)^n(n+1) = W_n(-1). \tag{68}$$

In addition, from the definition of the Chebyshev polynomials when $\cos\phi \neq 0$, one can also derive that

$$\sin(n\phi) = [\ W_n(\cos\phi) - T_n(\cos\phi)\ ] \cdot \tan\phi. \tag{69}$$

As a result, the stress formulas given by equations 30, 35, and 38 can be written in terms of Chebyshev polynomials. We demonstrate this for the general stress representation in equation 20, which can be written in terms of the Chebyshev polynomials as shown below:

$$\begin{aligned} s_i(n) \quad = \quad & f(n) * [\ b_{i,0}T_n(-1) + \sum_{k=1}^{\lfloor\frac{m}{2}\rfloor}(a_{i,k} - b_{i,k}\tan\theta_k)\cdot T_n(\cos\theta_k) + b_{i,k}\tan\theta_k \cdot W_n(\cos\theta_k)\ ] - \\ & -f(0)\cdot[\ b_{i,0}T_n(-1) + \sum_{k=1}^{\lfloor\frac{m}{2}\rfloor}(a_{i,k} - b_{i,k}\tan\theta_k)\cdot T_n(\cos\theta_k) + b_{i,k}\tan\theta_k \cdot W_n(\cos\theta_k)\ ], \end{aligned} \tag{70}$$

for $i = 1, 2, \ldots m$ and $n \geq 0$. This representation is valid when $\cos\theta_k \neq 0$ for all $1 \leq k \leq \lfloor\frac{m}{2}\rfloor$.

5. Conclusions

The resonance frequency spectrum in equation 15 of the discrete model was derived by developing an analytical representation for the stress solutions when a discrete sinusoidal forcing function was applied at one end of the strip while the other end was held fixed. The approach was based on the z-transform methods. Two key elements of this approach were that the determinant of the resulting global matrix $|\mathbf{A_m}|$ in the z-space was a palindromic polynomial with real coefficients and that its zeros were distinct and on the unit circle. An important connection was made in equation 15 between the angles ($\theta_0 = \pi$ and $\{\pm\theta_k\}_{k=1}^{\lfloor \frac{m}{2} \rfloor}$), representing the distinct zeros of $|\mathbf{A_m}|$ and the natural/resonance frequency spectrum. We showed that the resonance frequency spectrum in equation 15 for the discrete model consists of all the positive angles coterminal with $\theta_0 = \pi$, for m, odd only, and $\{\pm\theta_k\}_{k=1}^{\lfloor \frac{m}{2} \rfloor}$, for any m. It is important to notice that the positive angles coterminal with $\theta_0 = \pi$ represent resonance frequencies for any strip with an odd number of layers and do not depend on the material properties. According to equation 15, the resonance frequency spectrum for the discrete model depends only on (certain combinations of) the impedance ratios and not on any other parameters such as the length of the strip, etc. The design parameters representing such combinations for an m-layered strip were $\chi_{m-1} = \prod_{i=1}^{m-1} (1 + \alpha_i)$ for $2 \leq m \leq 5$ and Γ_{m-1} for $m = 4, 5$. This means that as long as m-layered designs with different impedance ratios have such design parameters in common, they are guaranteed to have the same resonance frequency spectrum for the discrete model.

The natural frequency spectrum of a free-fixed Goupillaud-type strip with up to five layers was first derived by simplifying and then solving the frequency equation. Independently of that, the linear transformation in frequency in equation 21 enabled us to heuristically describe the natural frequency spectrum of a free-fixed m-layered Goupillaud-type strip from the discrete model in equation 15. Both approaches provided an easy way to analytically describe the natural frequency spectrum versus solving the frequency equation directly. The frequency spectrum in equations 59 and appendix D, or appendix F, suggests that the natural frequency spectrum of a free-fixed m-layered Goupillaud-type strip depends only on (combinations of) the impedance ratios and (it is inversely proportional to) the equal wave travel time for each layer $\frac{\tau}{m}$. Designs with these quantities in common share the same natural frequency spectrum for the free-fixed boundary conditions (see subsections 3.3.1 and 3.3.2) and subsection 4.1 for illustrations of two different ways of obtaining such designs). A possible design modification that provides a desired natural frequency spectrum is also demonstrated in subsection 3.3.4.

When the resonance frequency results are combined with the stress optimization results obtained in Velo and Gazonas (*40*), we conclude that for a given optimal design of a Goupillaud-type layered strip with one fixed end, depending on the type of loading at the other end, one can get either the best or worst outcome when it comes to the stress amplitude. Although this work focused on a Goupillaud-type layered elastic strip, the frequency results were shown to extend to a non-Goupillaud-type layered strip. The stress formulas involving trigonometric sums were also interpreted using the Chebyshev polynomials of the first and second kind.

In this work, we have proven that the palindromic polynomial with real coefficients $|\mathbf{A_m}|$ has all its zeros on the unit circle for $1 \leq m \leq 5$, see appendix B. Whether this is true for any m-layered Goupillaud-type strip or only for certain classes of designs remains to be investigated. Proving rigorously/theoretically the conversion of the resonance frequency spectrum from the discrete model in equation 15 to the continuous model in equation 59 also remains to be shown. Finally, the experimental validation of the frequency results proposed here would be a natural and valuable extension of this work.

INTENTIONALLY LEFT BLANK.

6. References

1. Poisson, S. D. Mémoire sur l'équilibre et le Mouvement des Corps élastiques, Paris. *Paris, Mém. de l'Acad.* **1829**, *8* 357–570.

2. Lamb, H. On the Vibrations of an Elastic Sphere. *P. Lond. Math. Soc.* **1882**, *13* 189–212.

3. Love, A. E. H. *A Treatise on the Mathematical Theory of Elasticity*; 4^{th} ed.; Dover Publications: New York, 2002 (originally Cambridge University Press: 1927).

4. Ben-Menahem, A.; Singh, S. J. *Seismic Waves and Sources*; Springer-Verlag: New York, 1981.

5. Eringen, A. C.; Suhubi, E. S. *Elastodynamics, Vol. II, Linear Theory*; Academic Press: New York, 1975.

6. Nishida, K.; Kobayashi, N.; Fukao, Y. Resonant Oscillations Between Solid Earth and the Atmosphere. *Science* **2000**, *287* 2244–2246.

7. Brekhovskikh, L. M. *Waves in Layered Media*; Academic Press: New York, 1960.

8. Visscher, W. M.; Migliori, A.; Bell, T. M.; Reinert, R. A. On the Normal Modes of Free Vibration of Inhomogeneous and Anisotropic Elastic Objects. *J. Acous. Soc. Am.* **1991**, *90 (4)* 2154–2162.

9. Kosevich, A. M.; Minaev, P. A.; Syrkin, E. S. Interaction of Acoustic Waves with an Interface in Highly Anisotropic Layered Crystals. *Low Temp. Phys.* **2004**, *30 (6)* 500–504.

10. Ouchani, N.; Nougaoui, A.; Aynaou, H.; Bria, D.; El Boudouti, E. H.; Velasco, V. R.; Daoudi, A. Acoustic Waves in (110) Layered Structures. *Surf. Sci.* **2008**, *602* 2107–2113.

11. Fiorito, R.; Madigosky, W.; Uberall, H. Resonance Theory of Acoustic Waves Interacting with an Elastic Plate. *J. Acous. Soc. Am.* **1979**, *66 (6)* 1857–1866.

12. Jackins, P. D.; Gaunaurd, G. C. Resonance Acoustic Scattering from Stacks of Bonded Elastic Plates. *J. Acous. Soc. Am.* **1986**, *80 (6)* 1762–1776.

13. Mead, D. J. The Forced Vibration of One-Dimensional Multi-Coupled Periodic Structures: An Application to Finite Element Analysis. *J. Sound Vibrat.* **2009**, *319* 282–304.

14. Rao, M. K.; Scherbatiuk, K.; Desai, Y. M.; Shah, A. H. Natural Vibrations of Laminated and Sandwich Plates. *J. Eng. Mech.* **2004**, *130 (11)* 1268–1278.

15. Chandrashekara, S.; Santosh, U. An Efficient Solution to the Free Vibration of Thick Angle-ply Laminae. *Int. J. Solids Struct.* **1991**, *27 (8)* 999–1010.

16. Monsivais, G.; Rodriguez-Ramos, R.; Esquivel-Sirvent, R.; Fernandez-Alvarez, L. Stark-Ladder Resonances in Piezoelectric Composites. *Phys. Rev. B* **2003**, *68* 174109.

17. Ambati, M.; Fang, N.; Sun, C.; Zhang, X. Surface Resonant States and Superlensing in Acoustic Metamaterials. *Phys. Rev. B* **2007**, *75* 195447.

18. Wang, Z. G.; Lee, S. H.; Kim, C. K.; Park, C. M.; Nahm, K.; Nikitov, S. A. Effective Medium Theory of the One-Dimensional Resonance Phononic Crystal. *J. Phys.: Condens. Mat.* **2008**, *20* 055209.

19. Lange, K.; Rapp, B. E.; Rapp, M. Surface Acoustic Wave Biosensors: A Review. *Anal. Bioanal. Chem.* **2008**, *391* 1509–1519.

20. Leisure, R. G.; Willis, F. A. Resonant Ultrasound Spectroscopy. *J. Phys.: Condens. Mat.* **1997**, *9* 6001–6029.

21. Yang, J.; Yang, Z. Analytical and Numerical Modeling of Resonant Piezoelectric Devices in China-A Review. *Sci. China Ser. G* **2008**, *51 (12)* 1775–1807.

22. Abdulrehem, M. M.; Ott, E. Low Dimensional Description of Pedestrian-Induced Oscillation of the Millenium Bridge. *Chaos* **2009**, *19* 013129.

23. Broer, W.; Hoenders, B. J. Natural Modes and Resonances in a Dispersive Stratified N-Layer Medium. *J. Phys. A: Math. Theor.* **2009**, *42 (24)* 245207.

24. Fedorchenko, A. I.; Stachiv, I.; Wang, A. B.; Wang, W. H. Fundamental Frequencies of Mechanical Systems with N-Piecewise Constant Properties. *J. Sound Vibrat.* **2008**, *317* 490–495.

25. Hsueh, W. Analytical Solution of Harmonic Travelling Waves in N-segment Strings. *Proc. R. Soc. Lond. A* **2000**, *456* 2115–2126.

26. Gaudet, S.; Gauthier, C.; LeBlanc, V. G. On the Vibrations of an N-String. *J. Sound Vibrat.* **2000**, *238(1)* 147–169.

27. Churchill, R. R. *Operational Mathematics*; McGraw-Hill: New York, 1972.

28. Dhia, A. S. B. B.; Mercier, J. F. Resonances of an Elastic Plate in a Compressible Confined Fluid. *Q. J. Mech. Appl. Math.* **2007**, *60 (4)* 397–421.

29. Caviglia, G.; Morro, A. A Closed-Form Solution for Reflection and Transmission of Transient Waves in Multilayers. *J. Acous. Soc. Am.* **2004**, *116 (2)* 643–654.

30. Kaplunov, J.; Krynkin, A. Resonance Vibrations of an Elastic Interfacial Layer. *J. Sound Vibrat.* **2006**, *294* 663–677.

31. Qiang, G.; Wanxie, Z.; Howson, W. P. A Precise Method for Solving Wave Propagation Problems in Layered Anisotropic Media. *Wave Motion* **2004**, *40* 191–207.

32. Fokina, M. S.; Fokin, V. N. Resonances of Acoustic Waves Interacting with an Elastic Seabed. *J. Comput. Acoust.* **2001**, *9 (3)* 1079–1093.

33. Graff, K. F. *Wave Motion in Elastic Solids*; Dover Publications: New York, 1975.

34. Goupillaud, P. An Approach to Inverse Filtering of Near-Surface Layer Effects from Seismic Records. *Geophysics* **1961**, *36* 754–760.

35. Wang, N.; Lin, J. X.; Sadayuki, U. Goupillaud Inverse Problem with Arbitrary Input. *J. Acous. Soc. Am.* **1997**, *101 (6)* 3255–3260.

36. Knopoff, L. A Matrix Method for Elastic Wave Problems. *Bull. Seismol. Soc. Am.* **1964**, *54* 431–438.

37. Thomson, W. T. Transmission of Elastic Waves Through a Stratified Solid Medium. *J. Appl. Phys.* **1950**, *21* 89–93.

38. Haskell, N. A. The Dispersion of Surface Waves on Multilayered Media. *Bull. Seismol. Soc. Am.* **1953**, *43* 17–34.

39. Bube, K.; Burridge, R. The One Dimensional Inverse Problem of Reflection Seismology. *Siam Rev.* **1983**, *25 (4)* 497–559.

40. Velo, A. P.; Gazonas, G. A.; Ameya, T. z-Transform Methods for the Optimal Design of One-Dimensional Layered Elastic Media. *J. SIAM Appl. Math.* **2009**, *70* (3) 762–788.

41. Jury, E. I. *Theory and Application of the z-Transform Method*; John Wiley & Sons, Inc.: 1964.

42. Muir, T. *A Treatise on the Theory of Determinants*; Dover Publications: New York, 1960.

43. Proakis, J. G.; Manolakis, D. G. *Introduction to Digital Signal Processing*; Macmillan Publishing Company: 1988.

44. Spiegel, M. R.; Liu, J. *Mathematical Handbook of Formulas and Tables, Schaum's Outline Series*; 2nd Edition ed.; McGraw-Hill: 1999.

45. Ashby, M. F. *Materials Selection in Mechanical Design*; 2nd Edition ed.; Butterworth-Heinemann: Oxford, UK, 2000.

Appendix A. Stress Formulas for a Heaviside Loading

Some of the definitions and formulas in appendices A–E refer to the results from Velo and Gazonas (*40*). These results were obtained when studying stress propagation in a Goupillaud-type layered strip, subjected to zero initial conditions, a Heaviside step in stress loading $p = constant$ at time $t = 0$ at one end and held fixed at the other end. As before, the design parameters are given by $\chi_{m-1} = \prod_{i=1}^{m-1}(1+\alpha_i)$ for $2 \leq m \leq 5$, $\Gamma_3 = \alpha_1\alpha_3 - 1$, and $\Gamma_4 = \alpha_1\alpha_3\alpha_4 + \alpha_1\alpha_2\alpha_4 + \alpha_1\alpha_4 + \alpha_2\alpha_4 + \alpha_1\alpha_3 - 1$, where $\chi_{m-1} > 1$ for $m \geq 2$ and $\Gamma_{m-1} > -1$ for $m = 4, 5$. Here we recover from the general formulation in equations 5 and 9, the stress formulas derived in Velo and Gazonas (*40*) when the strip is subjected to a Heaviside step in stress loading p at time $t = 0$ on one end and held fixed on the other end. This case is illustrated in figure 1 for the choice of $f(n) = p$ for $n \geq 0$. Indeed, in this case we have $F(z) = Z(f(n)) = \frac{z}{z-1}p$ and $f(0) = p$, which imply that $(F(z) - f(0)) = \frac{p}{z-1}$. As a result, equation 9 becomes

$$\vec{x}_m = \frac{\eta_1 z(F(z)-f(0))}{|A_m|}\begin{bmatrix} |A_{1,1}| \\ -|A_{1,2}| \\ \vdots \\ (-1)^{1+m}|A_{1,m}| \end{bmatrix} = \frac{\eta_1 pz}{(z-1)|A_m|}\begin{bmatrix} |A_{1,1}| \\ -|A_{1,2}| \\ \vdots \\ (-1)^{1+m}|A_{1,m}| \end{bmatrix}, \qquad \text{(A-1)}$$

simplifies to,

$$\vec{x}_m(i) \;=\; \left[\, pz\tfrac{\eta_1(-1)^i|A_{1,i}|}{(z-1)|A_m|} \,\right] = pz\left[\, \tfrac{a_{i,0}}{z-1} + \tfrac{b_{i,0}}{z+1} + \sum_{k=1}^{\lfloor \frac{m}{2} \rfloor} \tfrac{a^*_{i,k}z + b^*_{i,k}}{z^2 - 2z\cos\theta_k + 1} \,\right]. \qquad \text{(A-2)}$$

After applying the inverse z-transform,

$$\begin{aligned} s_i(n) \;&=\; Z^{-1}(\vec{x}_m(i)) = Z^{-1}\left[\, \tfrac{a_{i,0}z}{z-1} + \tfrac{b_{i,0}z}{z+1} + \sum_{k=1}^{\lfloor \frac{m}{2} \rfloor} \tfrac{a^*_{i,k}z^2 + b^*_{i,k}z}{z^2 - 2z\cos\theta_k + 1} \,\right] \cdot p \\ &=\; Z^{-1}\left[\, \tfrac{a_{i,0}z}{z-1} + \tfrac{b_{i,0}\cdot\, z}{z+1} + \sum_{k=1}^{\lfloor \frac{m}{2} \rfloor} \left(\tfrac{a_{i,k}\cdot\, z(z-\cos\theta_k)}{z^2 - 2z\cos\theta_k + 1} + \tfrac{b_{i,k}\cdot z\sin\theta_k}{z^2 - 2z\cos\theta_k + 1} \right) \,\right] \cdot p, \end{aligned} \qquad \text{(A-3)}$$

the stress formulas follow,

$$s_i(n) = \left[a_{i,0} + b_{i,0}(-1)^n + \sum_{k=1}^{\lfloor \frac{m}{2} \rfloor} a_{i,k} \cos(n\theta_k) + b_{i,k} \sin(n\theta_k) \right] \cdot p, \tag{A-4}$$

for the choices of the coefficients given below

$$a_{i,k} = a^*_{i,k},\ b_{i,k} = \frac{a^*_{i,k} \cos\theta_k + b^*_{i,k}}{\sin\theta_k},\ \text{for } k = 1, \ldots, \lfloor \frac{m}{2} \rfloor. \tag{A-5}$$

As before, $\sin\theta_k \neq 0$ for all $k = 1, \ldots, \lfloor \frac{m}{2} \rfloor$ and $b_{i,0} = 0$ for m even. In addition, the trigonometric sums in the stress equations A-4, allow us to express them in terms of the Chebyshev polynomials of the first and second kind $T_n(y)$ and $W_n(y)$, by applying equation 68 and equation 69 as follows

$$s_i(n) = \left[a_{i,0} + b_{i,0} T_n(-1) + \sum_{k=1}^{\lfloor \frac{m}{2} \rfloor} (a_{i,k} - b_{i,k} \tan\theta_k) \cdot T_n(\cos\theta_k) + b_{i,k} \tan\theta_k \cdot W_n(\cos\theta_k) \right] \cdot p, \tag{A-6}$$

for $i = 1, 2, \ldots m$ and $n \geq 0$. This representation is valid when $\cos\theta_k \neq 0$ for all $1 \leq k \leq \lfloor \frac{m}{2} \rfloor$. The coefficients $a_{i,j}$, $b_{i,j}$, as well as the angles θ_k depend only on the impedance ratios α_i, $i = 1, 2, \ldots, m$, $j = 0, 1, \ldots, \lfloor \frac{m}{2} \rfloor$ and $k = 1, \ldots, \lfloor \frac{m}{2} \rfloor$.

Appendix B. Zeros of the Determinant $|\mathbf{A_m}|$

The expressions for the determinant $|\mathbf{A_m}|$ using the recursive equation 10 for $1 \leq m \leq 5$ are:

$$
\begin{array}{l}
|\mathbf{A_1}| = z+1, \;\; |\mathbf{A_2}| = (z+1)^2 - \eta_2\eta_1\alpha_1 z = z^2 - \frac{2(\chi_1-2)}{\chi_1}z + 1, \\
|\mathbf{A_3}| = (z+1)\cdot[\, z^2 - \frac{2(\chi_2-2)}{\chi_2}z + 1\,], \;\; |\mathbf{A_4}| = z^4 - \frac{4\Gamma_3}{\chi_3}z^3 + \frac{2(4\Gamma_3-\chi_3+8)}{\chi_3}z^2 - \frac{4\Gamma_3}{\chi_3}z + 1, \\
|\mathbf{A_5}| = (z+1)\cdot[\, z^4 - \frac{4\Gamma_4}{\chi_4}z^3 + \frac{2(4\Gamma_4-\chi_4+8)}{\chi_4}z^2 - \frac{4\Gamma_4}{\chi_4}z + 1\,].
\end{array}
\quad \text{(B-1)}
$$

The determinant $|\mathbf{A_m}|$ is a palindromic polynomial with real coefficients, as expected. All the zeros of $|\mathbf{A_m}|$ for $1 \leq m \leq 5$ are on the unit circle and distinct based on the following criteria.

1. The zeros of a quadratic factor with real coefficients of the form $z^2 + \mu z + 1$ are distinct (complex conjugate) on the unit circle iff $\mu^2 - 4 < 0$ or equivalently iff $|\mu| < 2$. When $m = 2, 3$ we have that $|\mu| < 2 \Leftrightarrow \left|\frac{\chi_{m-1}-2}{\chi_{m-1}}\right| < 1$, which is true because $\chi_{m-1} > 1$.

2. The zeros of a quartic factor with real coefficients of the form $z^4 + \mu z^3 + \nu z^2 + \mu z + 1$ are distinct (complex conjugate) on the unit circle [2] iff $[\, \mu^2 - 4\nu + 8 > 0$ and $|\frac{-\mu \pm \sqrt{\mu^2-4\nu+8}}{2}| < 2\,]$.

When $m = 4, 5$ we have the condition:

$\mu^2 - 4\nu + 8 > 0 \Leftrightarrow [\, (\chi_{m-1} - \Gamma_{m-1})^2 - 4\chi_{m-1}\,] = [\, (\Upsilon_{m-1} - 2)^2 - 4(1 + \Gamma_{m-1})\,] > 0$, where $\Upsilon_{m-1} = \chi_{m-1} - \Gamma_{m-1}$.

The inequality follows from the following relations:

$(\Upsilon_3 - 2)^2 - 4(1 + \Gamma_3) > (\alpha_1 + \alpha_3)^2 - 4\alpha_1\alpha_3 = (\alpha_1 - \alpha_3)^2 \geq 0$ for $m = 4$, and
$(\Upsilon_4 - 2)^2 - 4(1 + \Gamma_4) > (\alpha_1 + \alpha_2 + \alpha_1\alpha_2 + \alpha_3 + \alpha_4 + \alpha_3\alpha_4)^2 - 4(1 + \Gamma_4) >$
$(-\alpha_1 - \alpha_2 - \alpha_1\alpha_2 + \alpha_3 + \alpha_4 + \alpha_3\alpha_4)^2 \geq 0$ for $m = 5$.

The condition $\left|\frac{-\mu \pm \sqrt{\mu^2-4\nu+8}}{2}\right| < 2 \Leftrightarrow \left|\frac{\Gamma_{m-1} \pm \sqrt{(\chi_{m-1}-\Gamma_{m-1})^2-4\chi_{m-1}}}{\chi_{m-1}}\right| < 1$, which is true because $\chi_{m-1} > 1 > 0$ and $\Gamma_{m-1} + 1 > 0$ for $m = 4, 5$.

[2] This criterion is derived after dividing the quartic polynomial by z^2 and then applying the transformation $y = z + \frac{1}{z}$.

INTENTIONALLY LEFT BLANK.

Appendix C. Definition of the Matrix $\mathbf{D_m}$

The following equation is the definition of matrix $\mathbf{D_m}$:

$$\mathbf{D_m} = \begin{bmatrix} \mathbf{F} & \mathbf{B_1} & 0 & \dots & & & & & & \dots & 0 \\ \mathbf{C_2} & \mathbf{F} & \mathbf{B_2} & 0 & \dots & & & & & \dots & 0 \\ 0 & \mathbf{C_3} & \mathbf{F} & \mathbf{B_3} & 0 & \dots & & & & \dots & 0 \\ & \ddots & & \ddots & & \ddots & & & & & \\ 0 & \dots & & \dots & 0 & \mathbf{C_i} & \mathbf{F} & \mathbf{B_i} & 0 & \dots & 0 \\ & & & & & \ddots & & \ddots & \ddots & & 0 \\ 0 & \dots & & & & & \dots & 0 & \mathbf{C_{m-1}} & \mathbf{F} & \mathbf{B_{m-1}} \\ 0 & \dots & & & & & & \dots & 0 & \mathbf{C_m} & \mathbf{F} \end{bmatrix}_{2m \times 2m} \tag{C-1}$$

where $\mathbf{F} = \mathbf{I} + \mathbf{R^T},\ \mathbf{B_i} = \frac{4\alpha_i^2}{(1+\alpha_i)^2}\mathbf{I},\ \mathbf{C_i} = \frac{4}{(1+\alpha_i)^2}\mathbf{R^T},\ \mathbf{C_m} = 4\mathbf{R^T},\ \ 1 \leq i \leq m-1.$

Here θ represents any of the angles θ_j, $j = 0, \dots, \lfloor \frac{m}{2} \rfloor$, as applicable; $\mathbf{I}$ represents the 2×2 identity matrix; and $\mathbf{R^T}$ represents the transpose of the rotation matrix $\mathbf{R} = \begin{bmatrix} \cos\theta & -\sin\theta \\ \sin\theta & \cos\theta \end{bmatrix}$.

INTENTIONALLY LEFT BLANK.

Appendix D. Necessary Relations Among the Base Angles and Design Parameters

The angles identified here for a strip with up to five layers relate to the zeros of $|\mathbf{A_m}|$, already shown to be on the unit circle in appendix B. The $2\lfloor\frac{m}{2}\rfloor$ order equation for finding the non-trivial zeros of $|\mathbf{A_m}|$ in equation 13 is reduced to an $\lfloor\frac{m}{2}\rfloor$ order equation for the cosine of the base angles. The inequalities satisfied by the design parameters χ_{m-1} for $m = 2, 3$ and χ_{m-1}, Γ_{m-1} for $m = 4, 5$ in appendix B, validate the existence of these angles.

The two-layer case. The condition $|\mathbf{D_2}| = 0$ equivalent to $\left[\cos\theta - \frac{\chi_1-2}{\chi_1}\right]^2 = 0$, implies that

$$-1 < \cos\theta = \frac{\chi_1 - 2}{\chi_1} < 1 \implies 0 < \theta_1 = \cos^{-1}\left(\frac{\chi_1 - 2}{\chi_1}\right) < \pi, \tag{D-1}$$

The three-layer case. The condition $|\mathbf{D_3}| = 0$ is equivalent to $\left[\cos\theta = -1 \text{ or } \left(\cos\theta - \frac{\chi_2-2}{\chi_2}\right)^2 = 0\right]$, which based on the fact that $\chi_2 = (1+\alpha_1)(1+\alpha_2) > 1$, leads to the relations

$$\cos\theta = -1 \text{ or } -1 < \cos\theta = \frac{\chi_2 - 2}{\chi_2} < 1, \tag{D-2}$$

and the corresponding angle solutions

$$\theta_0 = \cos^{-1}(-1) = \pi, \quad 0 < \theta_1 = \cos^{-1}\left(\frac{\chi_2 - 2}{\chi_2}\right) < \pi. \tag{D-3}$$

The four-layer case. The condition $|\mathbf{D_4}| = 0 \Leftrightarrow [\chi_3\cos^2\theta - 2\Gamma_3\cos\theta + (2\Gamma_3 - \chi_3 + 4)]^2 = 0$, leads to the quadratic equation:

$$\cos^2\theta - \frac{2\Gamma_3}{\chi_3}\cos\theta + \frac{2\Gamma_3 - \chi_3 + 4}{\chi_3} = 0, \tag{D-4}$$

and implies the following base angle solutions for any given set of the design parameters χ_3 and Γ_3,

$$0 < \theta_{1,2} = \cos^{-1}\left(\frac{\Gamma_3 \pm \sqrt{(\chi_3 - \Gamma_3)^2 - 4\chi_3}}{\chi_3}\right) < \pi. \tag{D-5}$$

The five-layer case.
$|\mathbf{D_5}| = 0 \Leftrightarrow [\, \cos\theta = -1 \;$ or $[\, \chi_4 \cos^2\theta - 2\Gamma_4 \cos\theta + (2\Gamma_4 - \chi_4 + 4)\,]^2 = 0\,]$, leads to the equations:

$$\cos\theta = -1 \;\text{ or }\; \cos^2\theta - \frac{2\Gamma_4}{\chi_4}\cos\theta + \frac{2\Gamma_4 - \chi_4 + 4}{\chi_4} = 0, \tag{D-6}$$

and the corresponding angle solutions:

$$\theta_0 = \cos^{-1}(-1) = \pi, \quad 0 < \theta_{1,2} = \cos^{-1}\left(\frac{\Gamma_4 \pm \sqrt{(\chi_4 - \Gamma_4)^2 - 4\chi_4}}{\chi_4}\right) < \pi, \tag{D-7}$$

for any given set of the design parameters χ_4 and Γ_4.

Appendix E. Optimal Base Angles

For an m-layered Goupillaud-type elastic strip subjected to a Heaviside loading at one end and held fixed at the other end, the optimal designs have the smallest stress amplitude of double the loading. These optimal designs are characterized by the following optimal values of their base angles for $j = 2, 3, 4, \ldots$:

Table E-1. Optimal base angle values for the m-layer case.

m	**2**	**3**	**4**	**5**
Optimal Base Angles	$\theta_{1,opt} = \frac{\pi}{j}$	$\theta_{1,opt} = \frac{\pi}{2j-1}$	$\theta_{1,opt} = \frac{\pi}{2j}$, $\theta_{2,opt} = \pi - \frac{\pi}{2j}$	$\theta_{1,opt} = \frac{\pi}{2j+1}$, $\theta_{2,opt} = \frac{(2j-1)\pi}{2j+1}$

INTENTIONALLY LEFT BLANK.

Appendix F. Solutions of the Frequency Equations for a Free-fixed m-layered Goupillaud-type Elastic Strip ($2 \leq m \leq 5$)

F-1 Natural Frequency Spectrum for the Free-fixed Two-layer Case

After a few mathematical manipulations involving trigonometric identities, the frequency equation 57 for $m = 2$ becomes

$$\cos \tau\omega = \frac{\alpha_1 - 1}{\alpha_1 + 1} = \frac{\chi_1 - 2}{\chi_1}, \text{ where } \chi_1 = (1 + \alpha_1) > 1 \text{ or } \alpha_1 > 0. \tag{F-1}$$

This suggests the following natural frequency spectrum

$$\omega_{l_1} = \frac{1}{\tau} \cdot \left[\cos^{-1} \left(\frac{\chi_1 - 2}{\chi_1} \right) + 2l_1\pi \right], \ \omega_{l_2} = \frac{1}{\tau} \cdot \left[-\cos^{-1} \left(\frac{\chi_1 - 2}{\chi_1} \right) + 2(l_2 + 1)\pi \right] \tag{F-2}$$

for $l_1, l_2 = 0, 1, 2, \ldots$. Here α_1 represents the impedance ratio between the first and the second layer, while $\chi_1 = 1 + \alpha_1$. When both layers are occupied by the same material $(\alpha_1 = 1)$, equation F-1 recovers a known literature result for the natural frequency spectrum of a homogeneous strip of length τ given in Graff (*33*). In this case the frequency equation F-1 becomes $\cos \tau\omega = 0$, which implies the natural frequency spectrum $\omega_l = \frac{(2l+1)}{\tau} \cdot \frac{\pi}{2}$, $l = 0, 1, 2 \ldots$. Notice that equation F-1 implies that $\cos \tau\omega \neq \pm 1$.

F-2 Natural Frequency Spectrum for the Free-fixed Three-layer Case

Using the fact that $|\mathbf{\Delta_m}| = |\tilde{\mathbf{\Delta}}_\mathbf{m}|$, the frequency equation 57 for $m = 3$ becomes equivalent to solving the following equations:

$$\cos \frac{2\tau}{3}\omega = -1 \text{ or } \cos \frac{2\tau}{3}\omega = \frac{\chi_2 - 2}{\chi_2}, \text{ where } \chi_2 = (1 + \alpha_1)(1 + \alpha_2) > 1. \tag{F-3}$$

From equation F-3, the frequency spectrum for the three-layer is

$$\begin{cases} \omega_{l_0} = (2l_0 + 1)\frac{3\pi}{2\tau}, \\ \\ \omega_{l_1} = \frac{3}{2\tau} \cdot \left[\cos^{-1} \left(\frac{\chi_2 - 2}{\chi_2} \right) + 2l_1\pi \right], \ \omega_{l_2} = \frac{3}{2\tau} \cdot \left[-\cos^{-1} \left(\frac{\chi_2 - 2}{\chi_2} \right) + 2(l_2 + 1)\pi \right], \end{cases} \tag{F-4}$$

where $l_0, l_1, l_2 = 0, 1, 2, \ldots$.

F-3 Natural Frequency Spectrum for the Free-fixed Four-layer Case

Use of the double angle formula for the cosine for the four-layer case $(m = 4)$, results in $|\boldsymbol{\Delta_4}| = \frac{1}{4} \cdot \left[\chi_3 \cos^2 \frac{\tau}{2}\omega - 2\Gamma_3 \cos \frac{\tau}{2}\omega + (2\Gamma_3 - \chi_3 + 4)\right] = 0$, or equivalently

$$\cos^2 \frac{\tau}{2}\omega - \frac{2\Gamma_3}{\chi_3} \cos \frac{\tau}{2}\omega + \frac{2\Gamma_3 - \chi_3 + 4}{\chi_3} = 0. \tag{F-5}$$

For any given values of the design parameters χ_3 and Γ_3, the frequency spectrum is:

$$\begin{cases} \omega_{l_1} = \frac{2}{\tau} \cdot \left[\cos^{-1}\left(\frac{\Gamma_3 \pm \sqrt{(\chi_3 - \Gamma_3)^2 - 4\chi_3}}{\chi_3}\right) + 2l_1\pi\right], \\ \omega_{l_2} = \frac{2}{\tau} \cdot \left[-\cos^{-1}\left(\frac{\Gamma_3 \pm \sqrt{(\chi_3 - \Gamma_3)^2 - 4\chi_3}}{\chi_3}\right) + 2(l_2 + 1)\pi\right]. \end{cases} \quad l_1, l_2 = 0, 1, 2 \ldots, \tag{F-6}$$

When the first two layers are occupied by one material $(\alpha_1 = 1)$ and the other two are occupied by another material $(\alpha_2 \neq 1, \alpha_3 = 1)$, the four-layer case reduces to the two-layer case and equation F-5 reduces to equation F-1. From equation F-5 if follows that

$$\cos^2 \frac{\tau}{2}\omega = \frac{\alpha_2}{\alpha_2 + 1}, \tag{F-7}$$

which after applying the double angle formula for cosine becomes consistent with equation F-1,

$$\cos \tau\omega = \frac{\alpha_2 - 1}{\alpha_2 + 1}. \tag{F-8}$$

F-4 Natural Frequency Spectrum for the Free-fixed Five-layer Case

Similar to the previous cases, using symbolic algebra software and trigonometric identities we obtain for $m = 5$ that $|\boldsymbol{\Delta_5}| = \cos \frac{\tau\omega}{5} \cdot \left[\chi_4 \cos^4 \frac{\tau}{5}\omega - (\chi_4 + \Gamma_4) \cos^2 \frac{\tau}{5}\omega + (\Gamma_4 + 1)\right] = 0$. After using the double angle trigonometric formulas we have that

$$\cos \frac{2\tau}{5}\omega = -1 \text{ or } \cos^2 \frac{2\tau}{5}\omega - \frac{2\Gamma_4}{\chi_4} \cos \frac{2\tau}{5}\omega + \frac{2\Gamma_4 - \chi_4 + 4}{\chi_4} = 0. \tag{F-9}$$

The frequency spectrum can then be obtained for any given values of χ_4 and Γ_4.

Appendix G. Material Properties

The elastic modulus E and density ρ of the materials used in subsection 4.1 (see Ashby (*45*)) are as follows:

- Aluminum alloy: $E = 70$ GPa and $\rho = 2,500$ kg/m^3,
- Brass: $E = 20$ GPa and $\rho = 984.19$ kg/m^3,
- Bronze: $E = 50$ GPa and $\rho = 7,189.35$ kg/m^3,
- Copper alloy: $E = 10$ GPa and $\rho = 515.19$ kg/m^3,
- Glass fiber reinforced material: $E = 30$ GPa and $\rho = 1,130$ kg/m^3,
- Lead: $E = 14$ GPa and $\rho = 11,340$ kg/m^3,
- Nickel alloy: $E = 200$ GPa and $\rho = 348.18$ kg/m^3,
- Tungsten alloy: $E = 275$ GPa and $\rho = 19,610$ kg/m^3,
- Steel: $E = 200$ GPa and $\rho = 8,000$ kg/m^3.

INTENTIONALLY LEFT BLANK.

NO. OF COPIES	ORGANIZATION
1 (PDF ONLY)	DEFENSE TECHNICAL INFORMATION CTR DTIC OCA 8725 JOHN J KINGMAN RD STE 0944 FORT BELVOIR VA 22060-6218
1	DIRECTOR US ARMY RESEARCH LAB IMNE ALC HRR 2800 POWDER MILL RD ADELPHI MD 20783-1197
1	DIRECTOR US ARMY RESEARCH LAB RDRL CIM L 2800 POWDER MILL RD ADELPHI MD 20783-1197
1	DIRECTOR US ARMY RESEARCH LAB RDRL CIM P 2800 POWDER MILL RD ADELPHI MD 20783-1197
1	DIRECTOR US ARMY RESEARCH LAB RDRL D 2800 POWDER MILL RD ADELPHI MD 20783-1197
	ABERDEEN PROVING GROUND
1	DIR USARL RDRL CIM G (BLDG 4600)

NO. OF COPIES	ORGANIZATION
2	NSF S MCKNIGHT G PAULINO 4201 WILSON BLVD, STE 545 ARLINGTON, VA, 22230-0002
2	DARPA L CHRISTODOULOU W COBLENZ 3701 N FAIRFAX DR ARLINGTON VA 22203-1714
1	DIRECTOR US ARMY ARDEC AMSRD AAR AEE W E BAKER BLDG 3022 PICATINNY ARSENAL NJ 07806-5000
2	US ARMY TARDEC AMSTRA TR R MS 263 K BISHNOI D TEMPLETON MS 263 WARREN MI 48397-5000
1	COMMANDER US ARMY RSRCH OFC RDRL ROE N B LAMATTINA PO BOX 12211 RESEARCH TRIANGLE PARK NC 27709-2211
1	COMMANDER US ARMY RSRCH OFC RDRL ROI M J LAVERY PO BOX 12211 RESEARCH TRIANGLE PARK NC 27709-2211
1	COMMANDER US ARMY RSRCH OFC RDRL ROE M D STEPP PO BOX 12211 RESEARCH TRIANGLE PARK NC 27709-2211

NO. OF COPIES	ORGANIZATION
5	NAVAL RESEARCH LAB E R FRANCHI CODE 7100 M H ORR CODE 7120 J A BUCARO CODE 7130 J S PERKINS CODE 7140 S A CHIN BING CODE 7180 4555 OVERLOOK AVE SW WASHINGTON DC 20375
1	DTRA M GILTRUD 8725 JOHN J KINGMAN RD FORT BELVOIR VA 22060
1	ERDC US ARMY CORPS OF ENGINEERS USACEGSL P PAPADOS 7701 TELEGRAPH RD ALEXANDRIA VA 22315
1	AFOSR/NL 875 NORTH RANDOLPH ST SUITE 325, RM 3112 F FAHROO ARLINGTON VA 22203
1	CLEMSON UNIV DEPT MECH ENGINEERS M GRUJICIC 241 ENGRG INNOVATION BLDG CLEMSON SC 29634-0921
1	UNIV OF CALIFORNIA CTR OF EXCELLENCE FOR ADV MATLS S NEMAT NASSER SAN DIEGO CA 92093-0416
5	DIRECTOR LANL P MAUDLIN R GRAY W R THISSELL A ZUREK F ADDESSIO PO BOX 1663 LOS ALAMOS NM 87545

NO. OF COPIES ORGANIZATION

7 DIRECTOR
SANDIA NATL LABS
J BISHOP MS 0346
E S HERTEL JR MS 0382
W REINHART MS 1181
T VOGLER MS 1181
L CHHABILDAS MS 1811
M FURNISH MS 1168
M KIPP MS 0378
PO BOX 5800
ALBUQUERQUE NM 87185-0307

1 DIRECTOR
LLNL
M J MURPHY
PO BOX 808
LIVERMORE CA 94550

3 CALTECH
M ORTIZ MS 105 50
G RAVICHANDRAN
T J AHRENS MS 252 21
1201 E CALIFORNIA BLVD
PASADENA CA 91125

5 SOUTHWEST RSRCH INST
C ANDERSON
K DANNEMANN
T HOLMQUIST
G JOHNSON
J WALKER
PO DRAWER 28510
SAN ANTONIO TX 78284

1 TEXAS A&M UNIV
DEPT OF MATHEMATICS
J WALTON
COLLEGE STATION TX 77843

1 UNIVERSITY OF MISSISSIPPI
DEPT OF MECH ENGRG
A M RAJENDRAN
201-B CARRIER HALL
UNIVERSITY, MS 38677

2 SRI INTERNATIONAL
D CURRAN
D SHOCKEY
333 RAVENSWOOD AVE
MENLO PARK CA 94025

NO. OF COPIES ORGANIZATION

1 VIRGINIA POLYTECHNIC INST
COLLEGE OF ENGRG
R BATRA
BLACKSBURG VA 24061-0219

7 UNIV OF NEBRASKA
DEPT OF ENGRG MECH
F BOBARU
Y DZENIS
G GOGOS
M NEGAHBAN
R FENG
J TURNER
Z ZHANG
LINCOLN NE 68588

1 JOHNS HOPKINS UNIV
DEPT OF MECH ENGRG
K T RAMESH
LATROBE 122
BALTIMORE MD 21218

1 WORCESTER POLYTECHNIC INST
MATHEMATICAL SCI
K LURIE
WORCESTER MA 01609

4 UNIV OF UTAH
DEPT OF MATH
A CHERKAEV
E CHERKAEV
E S FOLIAS
R BRANNON
SALT LAKE CITY UT 84112

1 PENN STATE UNIV
DEPT OF ENGRG SCI & MECH
F COSTANZO
UNIVERSITY PARK PA 168023

4 UNIV OF DELAWARE
DEPT OF MECH ENGRG
T BUCHANAN
T W CHOU
A KARLSSON
M SANTARE
126 SPENCER LAB
NEWARK DE 19716

1 UNIV OF DELAWARE
CTR FOR COMPST MATRLS
J GILLESPIE
NEWARK DE 19716

NO. OF
COPIES ORGANIZATION

1 COMPUTATIONAL MECH CONSULTANTS
J A ZUKAS
PO BOX 11314
BALTIMORE MD 21239-0314

1 LOUISIANA STATE UNIV
R LIPTON
304 LOCKETT HALL
BATON ROUGE LA 70803-4918

1 INST OF ADVANCED TECH
UNIV OF TX AUSTIN
S BLESS
3925 W BRAKER LN STE 400
AUSTIN TX 78759-5316

1 APPLIED RSCH ASSOCIATES
D E GRADY
4300 SAN MATEO BLVD NE
STE A220
ALBUQUERQUE NM 87110

1 INTERNATIONAL RSRCH ASSOC INC
D L ORPHAL
4450 BLACK AVE
PLEASANTON CA 94566

3 ORNL
ENVIRONMENTAL SCI DIV
W DOLL
T GAMEY
L BEARD
PO BOX 2008
OAK RIDGE TN 37831

2 WASHINGTON ST UNIV
INST OF SHOCK PHYSICS
Y M GUPTA
J ASAY
PULLMAN WA 99164-2814

1 NORTHWESTERN UNIV
DEPT OF CIVIL & ENVIRON ENGRG
Z BAZANT
2145 SHERIDAN RD A135
EVANSTON IL 60208-3109

1 UNIV OF DAYTON
RSRCH INST
N S BRAR
300 COLLEGE PARK
MS SPC 1911
DAYTON OH 45469

2 TEXAS A&M UNIV
DEPT OF GEOPHYSICS MS 3115
F CHESTER
T GANGI
COLLEGE STATION TX 778431

1 UNIV OF SAN DIEGO
DEPT OF MATH & CMPTR SCI
A VELO
5998 ALCALA PARK
SAN DIEGO CA 92110

1 NATIONAL INST OF STANDARDS & TECHLGY
BLDG & FIRE RSRCH LAB
J MAIN
100 BUREAU DR MS 8611
GAITHERSBURG MD 20899-8611

1 MIT
DEPT ARNTCS ASTRNTCS
R RADOVITZKY
77 MASSACHUSETTS AVE
CAMBRIDGE MA 02139

1 UNIV OF DELAWARE
DEPT ELECTRICAL & CMPTR ENGRG
D WEILE
NEWARK DE 19716

1 T W WRIGHT
4906 WILMSLOW RD
BALTIMORE MD 21210

1 UNIV OF TEXAS-PAN AMERICAN
COLLEGE OF ENGRG
& COMPUTER SCI
D H ALLEN
1201 WEST UNIVERSITY DR
EDINBURG, TX 78539-2999

3 RDRL D
J CHANG
R SKAGGS
V WEISS
BLDG 205
2800 POWDER MILL RD
ADELPHI MD 20783-1197

ABERDEEN PROVING GROUND

76 DIR USARL

NO. OF COPIES	ORGANIZATION
	RDRL WM
	B FORCH
	S KARNA
	J MCCAULEY
	P PLOSTINS
	M ZOLTOSKI
	RDRL WML
	D LYONS
	J NEWILL
	RDRL WML B
	I BATYREV
	B RICE
	N WEINGARTEN
	RDRL WML D
	P CONROY
	M NUSCA
	RDRL WML G
	M BERMAN
	W DRYSDALE
	RDRL WML H
	D SCHEFFLER
	S SCHRAML
	B SCHUSTER
	RDRL WMM
	J BEATTY
	R DOWDING
	J ZABINSKI
	RDRL WMM A
	M MAHER
	J TZENG
	E WETZEL
	RDRL WMM B
	T BOGETTI
	B CHEESEMAN
	C FOUNTZOULAS
	A GAZONAS
	G GAZONAS
	D HOPKINS
	P MOY
	B POWERS
	C RANDOW
	T SANO
	M VANLANDINGHAM
	R WILDMAN
	C F YEN
	RDRL WMM C
	J LA SCALA
	RDRL WMM D
	E CHIN
	K CHO
	RDRL WMM E
	M COLE
	T JESSEN
	J LASALVIA
	M PEPI
	J SANDS
	RDRL WMM F
	L KECSKES
	H MAUPIN
	RDRL WML G
	J ANDZELM
	A RAWLETT
	RDRL WMP
	P BAKER
	S SCHOENFELD
	RDRL WMP B
	R BECKER
	S BILYK
	D CASEM
	J CLAYTON
	M GREENFIELD
	C HOPPEL
	R KRAFT
	B LEAVY
	B LOVE
	M RAFTENBERG
	M SCHEIDLER
	T WEERASOOYIA
	RDRL WMP C
	T BJERKE
	S SEGLETES
	RDRL WMP D
	R DONEY
	J RUNYEON
	B SCOTT
	RDRL WMP E
	M BURKINS
	RDRL WMP F
	M CHOWDHURY
	A FRYDMAN
	N GNIAZDOWSKI
	R GUPTA
	RDRL WMP G
	N ELDREDGE
	D KOOKER
	S KUKUCK
	G R PEHRSON

INTENTIONALLY LEFT BLANK.